

INVESTIGATING THE OPTICAL PROPERTIES OF $\text{Cd}_{1-x}\text{Zn}_x\text{S}$ THIN FILMS DEPOSITED
BY THE DIP TECHNIQUE

BY

KNUST

DAVID OMPONG BSc.Physics (Hons.)

A Thesis submitted to the Department of Physics, Kwame Nkrumah University of
Science and Technology, in partial fulfillment of the requirement for the degree of

MASTER OF SCIENCE (SOLID STATE PHYSICS)

Faculty of Physical Sciences,

College of Science

FEBRUARY, 2010

DECLARATION

I hereby declare that this submission is my own work towards the M.Sc. and that, to the best of my knowledge, it contains no material previously published by any person nor material which has been accepted for the award of any other degree of the University, except where due acknowledgment has been made in the text.

KNUST

David Ompong

.....

Student

.....

Signature

.....

Date

Certify by;

Prof. F. Boakye

.....

Supervisor

.....

Signature

.....

Date

Certify by;

Dr. S. K. Danuor

.....

Head of Department

.....

Signature

.....

Date

ACKNOWLEDEMENT

I take this opportunity to thank all the people who have helped me and who continue to inspire me.

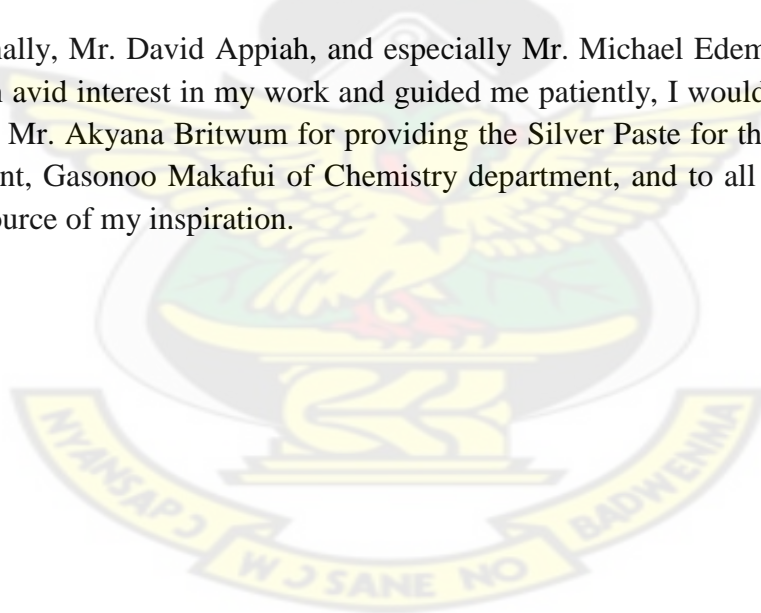
My deepest appreciation and gratitude is dedicated to my research supervisor, Professor Francis Boakye. I recognize that he is a preeminent professor in the field of solid state physics at the department as well as being a good person, providing me continuous support and guidance along the whole way of this research work.

I want to extend my heartfelt thanks to Dr. S.K. Twumasi of chemistry department, KNUST, for the assistance he offered on the sample preparation techniques and also for useful discussions related to the research.

My thanks also go to Mr. Kofi Ampong, Mr. Acheampong Aning, and Mr. Asare Van-Dycke for their immense support and encouragement to me during this work.

Last but not least, am grateful to Mr. Teddy Delali Blutse, technical instructors at the Department of Biochemistry, KNUST-Kumasi.

Finally, Mr. David Appiah, and especially Mr. Michael Edem Donkor, who have shown an avid interest in my work and guided me patiently, I would like to give special thanks to Mr. Akyana Britwum for providing the Silver Paste for the Photoconductivity experiment, Gasonoo Makafui of Chemistry department, and to all my colleagues, you are the source of my inspiration.



ABSTRACT

Thin films of $\text{Cd}_{1-x}\text{Zn}_x\text{S}$ ternary alloy have been prepared by the dip technique using thiourea and the nitrates of cadmium and zinc. The optical properties have been investigated by spectrophotometry and photoconductivity studies. The calculated film thickness using the gravimetric method were $18.85\mu\text{m}$, $8.61\mu\text{m}$, $5.06\mu\text{m}$, $6.23\mu\text{m}$ for $x= 0.2, 0.4, 0.6, 0.8$ respectively. The absorption spectra, $A(\lambda)$, of the films at normal incidence of light were obtained in the spectral region 300–900 nm using LKB ultraspecII 4050 UV/Visible spectrophotometer. The optical band gap of the as deposited films varied from 2.42eV ($x =0.2$) to 3.61eV ($x =0.8$), that is, the band gap increased with increasing Zn concentration of the alloy. The as deposited samples were thermally annealed in air for about an hour at temperatures of 100°C, 200°C and 300°C and the absorption spectra again recorded. It was revealed that thermal annealing decreased the optical band gap; this may be due to improved crystalline structure of the samples as a result of the heat treatment. The average extinction coefficient for the as deposited samples were 6.89×10^{-3} , 10.27×10^{-3} , 19.93×10^{-3} , 22.16×10^{-3} for $x= 0.2, 0.4, 0.6, 0.8$ respectively. The films formed were moderately photoconductive in the as deposited state with photocurrent peaking at 98 μA in the $\text{Cd}_{0.8}\text{Zn}_{0.2}\text{S}$ sample. The photocurrent decreased as Zn content increased in the solution. The $\text{Cd}_{0.8}\text{Zn}_{0.2}\text{S}$ film showed a high photoconductivity around 2.20 eV. This energy was quite close but smaller than the corresponding band gap of 2.42 eV of the sample with a difference of 0.22 eV. Transition from localized states within the forbidden gap is speculated to be the cause for the photoconductivity.

TABLE OF CONTENTS

	PAGE
Title page	i
Declaration	ii
Acknowledgement	iii
Abstract	iv
Table of contents	v
List of figures	ix
List of tables	xii
Abbreviations and acronyms	xiii

CHAPTER ONE

1. INTRODUCTION.....	1
1.0. GENERAL INTRODUCTION.....	1
1.1. OBJECTIVES OF PROJECT	4
1.1.1. SPECIFIC OBJECTIVES OF PROJECT.....	5
1.2. STRUCTURE OF THESIS	6

CHAPTER TWO

2. LITERATURE REVIEW.....	7
2.0. SEMICONDUCTOR ALLOYS.....	7
2.1. WHY THE INTEREST IN $Cd_{1-x}Zn_xS$	7
2.2. ELECTRICAL, OPTICAL AND STRUCTURAL	

CHARACTERIZATION OF $Cd_{1-x}Zn_xS$	8
2.3. LOW DIMENSIONAL $Cd_{1-x}Zn_xS$	19
2.4. BASICS OF FILM FORMATION AND STRUCTURE.....	23
2.5. ANNEALING.....	26
2.5.1. IRRADIATION ANNEALING.....	27
2.5.2. RECRYSTALLIZATION ANNEALING.....	27
2.5.3. PULSED ANNEALING OF SEMICONDUCTORS.....	28

CHAPTER THREE

3. THEORITICAL BACKGROUND.....	29
3.0. CLASSIFICATION OF SOLIDS.....	29
3.0.1. CRYSTALLINE SEMICONDUCTORS.....	30
3.0.2. POLYCRYSTALLINE SEMICONDUCTORS.....	31
3.0.3. AMORPHOUS SEMIC ONDUCTORS.....	33
3.1. OPTICAL PROPERTIES OF FILM MATERIALS.....	37
3.1.1. OPTICAL MAGNITUDES AND THE DIELECTRIC CONSTANTS.....	40
3.1.2. ELCTRONIC TRANSITIONS IN SEMICONDUCTORS.....	42
3.1.3. IMPURITY ABSORPTION.....	43
3.1.4. OPTICAL ABSORPTION AND BAND GAP.....	44
3.2. THE PHOTOCONDUCTIVITY EFFECT.....	45

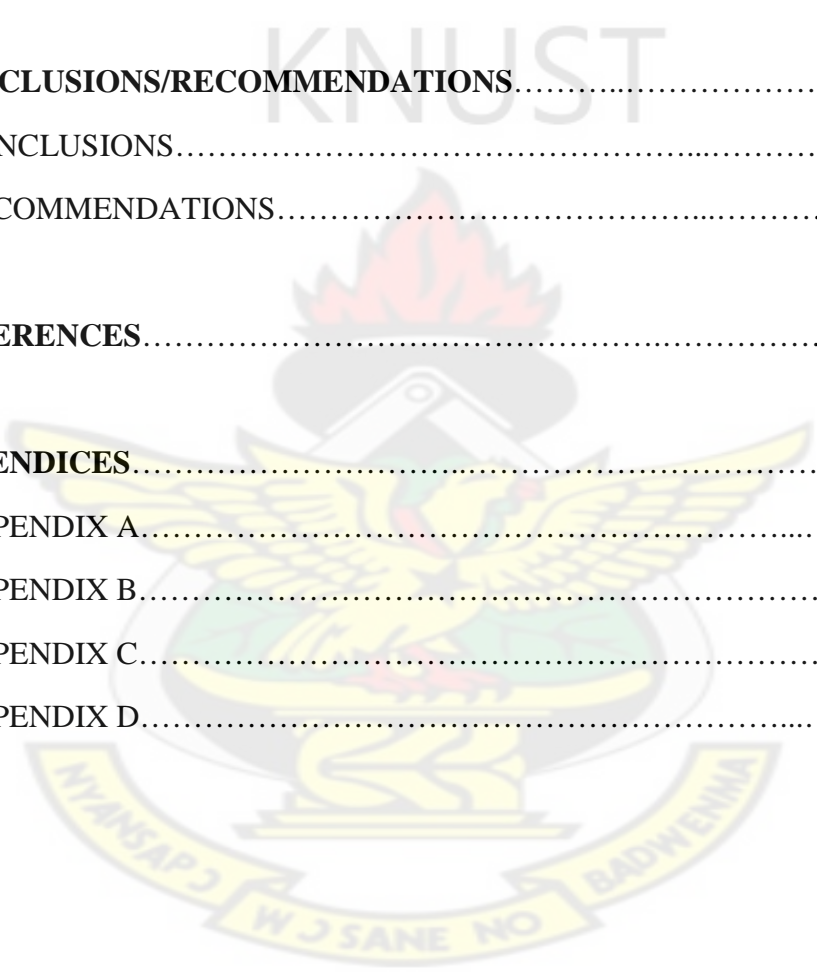
CHAPTER FOUR

4. EXPERIMENTAL DETAILS.....	50
4.0. REAGENTS.....	50
4.0.1. 0.25M ZINC NITRATE SOLUTION (Zn(NO ₃) ₂).....	50
4.0.2. 1.0 M CADMIUM NITRATE SOLUTION (Cd(NO ₃) ₂).....	50
4.0.3. 0.375 M CADMIUM NITRATE SOLUTION (Cd(NO ₃) ₂).....	50
4.0.4. 0.1667 M CADMIUM NITRATE SOLUTION (Cd(NO ₃) ₂).....	51
4.0.5. 0.0625 M CADMIUM NITRATE SOLUTION (Cd(NO ₃) ₂).....	51
4.0.6. 0.5M THIOUREA SOLUTION ((NH ₂) ₂ CS).....	51
4.1. SURFACE PREPARATION OF SUBSTRATES.....	51
4.2. SAMPLE PREPARATION.....	52
4.3. THE MEASUREMENT OF ABSORPTION SPECTRA.....	54
4.4. THE MEASUREMENT OF FILM THICKNESS.....	55
4.5. PHOTOCONDUCTIVITY TEST.....	57

CHAPTER FIVE

5. RESULTS AND DISCUSSION.....	59
---------------------------------------	-----------

5.0. VARIATION OF ABSORPTION COEFFICIENT VERSUS ENERGY AT DIFFERENT ANNEALING TEMPERATURES.....	59
5.1. OPTICAL BAND GAP	61
5.2. VARIATION OF EXTINCTION COEFFICIENT WITH WAVELENGTH.....	67
5.3. PHOTOCONDUCTIVITY RESULTS.....	67
6. CONCLUSIONS/RECOMMENDATIONS.....	71
6.0. CONCLUSIONS.....	71
6.1. RECOMMENDATIONS.....	72
7. REFERENCES.....	73
8. APPENDICES.....	77
8.0. APPENDIX A.....	77
8.1. APPENDIX B.....	84
8.2. APPENDIX C.....	85
8.3. APPENDIX D.....	88



LIST OF FIGURES

<u>FIGURE</u>		<u>PAGE</u>
Figure 2.1	Resistivity data for some CdZnS films.....	16
Figure 2.2	XRD patterns of (a) CdS, (b) Zn/CdS structure exposed to thermal annealing at 570 °C for 5 min; (c) fragment of (a) and (b) patterns for $2\theta = 26-30^\circ$	18
Figure 2.3	Variation of optical absorption coefficient (α) with photon energy ($h\nu$) for different compositions (x value) of $Cd_{1-x}Zn_xS$ films.....	21
Figure 2.4	plot of $(\alpha h\nu)^2$ vs. $h\nu$ for four different compositions: (a) $x = 0$, (b) $x = 0.4$, (c) $x = 0.6$ and (d) $x = 1$	22
Figure 2.5	Basic modes of thin film growth.....	25
Figure 3.1	Schematics of the three general types of structural orders: (a) amorphous, (b) polycrystalline, (c) crystalline.....	29
Figure 3.2	Area of mobility between valence and conduction bands.....	35
Figure 3.3	Schematic illustration of a two-dimensional continuous random network of atoms having various bonding coordination.....	36
Figure 3.4	Absorption coefficient is plotted as a function of the photon energy in typical semiconductor to illustrate various possible absorption processes.....	39
Figure 3.5a	Direct electron transition in semiconductor with accompanying photon emission.....	43

Figure 3.5b	Indirect electron transition in semiconductor via a defect level.....	43
Figure 3.6	Photoconductivity process in a semiconductor specimen.....	48
Figure 4.1	Experimental set-up for thin film deposition by the dip technique.....	53
Figure 4.2	Schematic diagram of a single-beam spectrophotometer.....	55
Figure 4.3	Schematic diagram of photoconductivity set-up.....	58
Figure 5.1	Absorption coefficient, α , versus photon energy, $h\nu$, for $\text{Cd}_{0.8}\text{Zn}_{0.2}\text{S}$ sample.....	60
Figure 5.2	Absorption coefficient, α , versus photon energy, $h\nu$, for $\text{Cd}_{0.6}\text{Zn}_{0.4}\text{S}$ sample.....	60
Figure 5.3	Square of absorption coefficient, α^2 , multiplied by square of photon energy, $(h\nu)^2$, plotted as a function of the photon energy, $h\nu$, for $\text{Cd}_{0.8}\text{Zn}_{0.2}\text{S}$ film annealed at different temperatures.....	62
Figure 5.4	Square of absorption coefficient, α^2 , multiplied by square of photon energy, $(h\nu)^2$, plotted as a function of the photon energy, $h\nu$, for $\text{Cd}_{0.6}\text{Zn}_{0.4}\text{S}$ film annealed at different temperatures.....	64
Figure 5.5	A plot of transmittance versus wavelength.....	64
Figure 5.6	Square of absorption coefficient, α^2 , multiplied by square of photon energy, $(h\nu)^2$, plotted as a function of the photon energy, $h\nu$, for $\text{Cd}_{0.4}\text{Zn}_{0.6}\text{S}$ film annealed at different temperatures.....	65
Figure 5.7	Optical band gap variation with zinc concentration in the samples.....	65
Figure 5.8	A plot of extinction coefficient versus wavelength for $\text{Cd}_{0.4}\text{Zn}_{0.6}\text{S}$ sample.....	66
Figure 5.9	A plot of extinction coefficient versus wavelength for	

	Cd _{0.2} Zn _{0.8} S sample.....	66
Figure 5.10	A plot of photocurrent versus time for the sample Cd _{0.8} Zn _{0.2} S.....	68
Figure 5.11	A plot of photocurrent versus time for the sample Cd _{0.4} Zn _{0.6} S.....	68
Figure 5.12	A plot of photocurrent versus photon energy for the sample Cd _{0.8} Zn _{0.2} S.....	69
Figure 5.13	A plot of photocurrent versus photon energy for the sample Cd _{0.6} Zn _{0.4} S.....	69
Figure C1	Absorption coefficient, α , versus photon energy, $h\nu$, for Cd _{0.4} Zn _{0.6} S sample.....	85
Figure C2	Absorption coefficient, α , versus photon energy, $h\nu$, for Cd _{0.2} Zn _{0.8} S sample.....	85
Figure C3	Square of absorption coefficient, α^2 , multiplied by square of photon energy, ($h\nu$) ² , plotted as a function of the photon energy, $h\nu$, for Cd _{0.2} Zn _{0.8} S film annealed at different temperatures.....	86
Figure C4	A plot of extinction coefficient versus wavelength for Cd _{0.8} Zn _{0.2} S sample.....	87
Figure C5	A plot of extinction coefficient versus wavelength for Cd _{0.6} Zn _{0.4} S sample.....	87

LIST OF TABLES

<u>TABLE</u>	<u>PAGE</u>
Table 1.1. Combination of the various ions concentrations employed in the preparation of the samples.....	52
Table 1.2. A summary of selected film thickness measurement techniques.....	56
Table 5.1. Absorbance reading for as deposited films.....	77
Table 5.2. Absorbance reading for films annealed at 100 °C.....	78
Table 5.3. Absorbance reading for films annealed at 200 °C.....	80
Table 5.4. Absorbance reading for films annealed at 300 °C.....	81
Table 5.5. Variation of sample composition with optical band gaps evaluated from absorption spectra.....	84
Table 5.6. Energy gap for III-V, II-VI, I-VII semiconductors at room temperature	84

KNUST

ABBREVIATIONS AND ACRONYMS

A	Absorbance
α	Absorption coefficient
BDH	British Drug House
CBD	Chemical Bath Deposition
CdTe	Cadmium Telluride
(Cd, Zn)S	Cadmium Zinc Sulfide
CdO	Cadmium Oxide
CdS	Cadmium Sulfide
CGS	Copper-Gallium-Selenide
CIS	Copper-Indium-Selenide
CIGS	Copper-Indium-Gallium-Selenide
CSS	Close Spaced Sublimation
CVD	Chemical Vapor Deposition
DOS	Density of States
ED	Electron Diffraction
EDXRF	Energy Dispersive X-Ray Fluorescence
h	Planck constant
HP	Hewlett-Packard

IR	Infrared
<i>k</i>	Wave vector, Extinction coefficient
λ	Wavelength
M	Molar concentration
MBE	Molecular Beam Epitaxy
P	Film Packing Factor
<i>P(r)</i>	Radial distribution function
ρ	Resistivity
SEM	Scanning Electron Microscopy
T	Transmittance
TEA	Triethanolamine
τ_h	Heating time
τ_c	Cooling time
UV	Ultraviolet
ν	Photon frequency
VIS	Visible Spectrum
<i>x, y</i>	Compositional parameters/an integer number in polyacetylene
XRD	X-Ray Diffraction
ZnS	Zinc Sulfide

CHAPTER ONE

1.0. GENERAL INTRODUCTION

During the recent decades, advances in semiconductor materials resulted in the development of a wide range of electronic and optoelectronic devices that affected many aspects of the technological society. From semiconductors to microelectronic and optoelectronic devices for information applications, these advances and applications were catalyzed by an improved understanding of the interrelationship between different aspects (i.e., structure, properties, synthesis and processing, performance, and characterization of materials) of this multidisciplinary field (Yacobi, B.G., 2004).

Starting with the development of the transistor by John Bardeen, Walter Brattain and William Shockley at Bell Telephone Laboratories in 1947, the technology of semiconductors has exploded. With the creation of integrated circuits and chips, semiconductor devices have penetrated into large parts of our lives. The modern desktop or laptop computer would be unthinkable without microelectronic semiconductor devices, and so would a myriad of other devices (Pettersen, J. D. and Bailey, B. C., 2005).

Semiconductors are usually crystalline solids although liquid and amorphous semiconductors are also known. They have electrical resistivity which is intermediate between that of metals and insulators which decrease usually exponentially, with temperature (Juster, N. J., 1963). Semiconductors can be distinguished from other materials by a number of physical properties, one of the most important of which is the electrical resistivity ρ or the difficulty with which an electric current can pass through the material under the influence of an electric field. Materials can be classified into three

categories: insulators, for which the resistivity is very high (10^{12} $\Omega\cdot\text{cm}$); metals, for which the resistivity is very low (10^{-6} $\Omega\cdot\text{cm}$); and semiconductors, for which the resistivity is intermediate in value (10^6 - 10^3 $\Omega\cdot\text{cm}$) and is highly temperature dependent. The temperature dependences of the resistivities of metals and semiconductors are quite different. For metals the temperature dependence is typically weak and the resistivity increases with increasing temperature. For semiconductors the opposite is typically the case. The temperature dependence is strong and the resistivity for the most part decreases with increasing temperature (Balkanski, M. and Wallis, R.F., 2000). It should be noted, however, that for semiconductors the boundaries for both the resistivity (between about 10^{-3} and 10^9 $\Omega\cdot\text{cm}$) and the upper limit of the energy gap (of about 4 eV) are only approximate. For example, diamond, having the energy gap of about 5.5 eV also exhibit semiconducting properties if properly processed (e.g., doped) for applications in semiconductor devices (Yacobi, B.G., 2004).

Two general classifications of semiconductors are the elemental semiconductor materials, found in group IV of the periodic table (see appendix D), and compound semiconductor materials (Neamen, D.A., 2003). Some examples of common semiconductors that are widely used in electronic and optoelectronic applications are group IV elemental semiconductors (e.g., Si and Ge), group III-V semiconductor compounds (e.g., AlAs, GaAs, GaP, GaN, InP, and InSb), group II-VI compounds (e.g., ZnS, ZnSe, ZnTe, CdS, CdSe, and CdTe), and group IV-VI compounds (e.g., PbS, PbSe, and PbTe). In addition to these elemental and binary semiconductors, materials such as ternary (e.g., $\text{Al}_x\text{Ga}_{1-x}\text{As}$, $\text{GaAs}_{1-x}\text{P}_x$, and $(\text{Hg}_{1-x}\text{Cd}_x\text{Te})$) and quaternary (e.g., $\text{Ga}_x\text{In}_{1-x}\text{As}_y\text{P}_{1-y}$) alloys with “tunable” (adjustable) properties are also used in specific device applications. The subscript x and y are composition parameters. Organic compounds

which are semiconductors include anthracene, $C_{14}H_{10}$, and polyacetylene $(CH)_x$ (Yacobi, B.G., 2004; Balkanski, M. and Wallis, R.F., 2000). This thesis is primarily concerned with the optical studies on the group II-VI semiconductor ternary alloy, cadmium zinc sulphide $Cd_{1-x}Zn_xS$ thin films deposited by the dip technique.

Generally speaking, semiconductor research in the true sense began with the application of quantum theory to the solid state through the studies of Heisenberg, Sommerfeld, Fermi and others in 1928; the specific application to semiconductors and the energy level picture was made by Wilson in 1930. An even greater stimulus to research was given by the invention of the transistor. Because of the tremendous practical importance of the electrical properties of semiconductors, theory and practice have always gone hand in hand in this field (Dunlap, W.C., 1961).

In addition to being very important for material science, the study of semiconductors is of great interest for fundamental research as well, as a great number of new phenomena can be observed in them. For example, the discovery of the quantum Hall effect arose from the possibility of creating semiconductor heterojunctions in which the electron gas is practically confined to a two-dimensional region next to the interface. This opened the way to the study of the properties rooted in the two-dimensional character of the system. Besides, very high purity materials can be fabricated from a semiconductor, which is a prerequisite to studying certain physical phenomena (Sólyom, J., 2008).

The growing importance of semiconductor devices is leading to even more challenging problems of fabrication to produce better, cheaper, and more reliable devices. Inorganic salts in the form of thin films should be much easier to incorporate into practical device structures. The problem of miniaturization and multiplexing of

devices have challenged the knowledge of fabrication techniques as well as the materials themselves to an extent which has kept researchers in this field busy for years.

As sophistication grows in this field, “molecular engineering” looms over the horizon as the ultimate challenge in this field, fusing the problems of materials fabrication, device research, and systems design into a single integrated problem.

Although much has been learnt in the past about the physics of semiconductors, new developments are still coming thick and fast and in the materials area there is still tremendous need for progress. For many applications and to observe many interesting properties semiconductor must be prepared with a purity and structural perfection greatly exceeding that attainable in other materials. To produce transistor action, for example, silicon and germanium purer and more perfect than any other known materials are regularly being manufactured for commercial production (Dunlap, W.C., 1961).

1.1. OBJECTIVES OF PROJECT

Cadmium base binary and ternary II-VI compound semiconductors have attracted considerable interest because of their wide applications in optoelectronic devices (Panin *et al.*, 1998). Interest in the preparation and study of the physical properties of ternary chalcogenide compounds for their possible application in solar cells, light emitting diodes and non-linear optical devices has been increasing in recent years (Ortega-Lopez *et al.*, 2003). Ternary compounds are found to be promising materials for optoelectronic device applications such as green light emitting devices and are suggested to be possible material for window layer of solar cells. These compounds are increasingly being studied for efficient solar energy conversion through photo-electrochemical solar cells

and have become potential candidate for such applications (Woon-Jo and Gye-Choon, 2003; Padam, G.K and Rao, S.U.M., 1986; Pawar *et al.*, 1986).

Although, much research has been done on (Cd, Zn)S thin films and their applications in optoelectronic devices, very little has been reported on how thermal annealing affects the optical properties of (Cd, Zn)S thin films prepared using the dip technique. Knowledge of the optical band gap, refractive index, extinction coefficient, transmittance and absorbance of a material are essential in characterizing materials for optoelectronic device fabrication. Also, being able to 'tune' the optical properties can result in materials for specific application.

For instance, fabricating good $\text{CuIn}_{1-x}\text{Ga}_x\text{Se}_2$ (CIGS) p-n junction solar cells requires selecting an n-type buffer layer material with a lattice parameter that is well matched to the absorber layer as well as having favorable band offsets. Cadmium Zinc Sulphide ternary material with wurtzite structure fits this application (AbuShama, J. R., *et al.*, 2005), yet still being able to tune the optical properties of $\text{Cd}_{1-x}\text{Zn}_x\text{S}$ thin film by thermally annealing it or varying the relative ratio of cadmium and zinc may make it fit buffer layer material with enhanced performance. Studying the photoconductive properties of the films will also throw more light on the nature of electronic transition ongoing in this alloy.

1.1.1. SPECIFIC OBJECTIVES OF PROJECT

Accordingly, the research presented in this thesis was motivated by the following objectives:

- To investigate the optical properties of $\text{Cd}_{1-x}\text{Zn}_x\text{S}$ thin films deposited by the dip technique.

- To study the effect of thermal annealing on the optical properties of $\text{Cd}_{1-x}\text{Zn}_x\text{S}$ thin films.
- Photoconductivity studies will be conducted on the samples as well to support the spectrophotometric studies.

1.2. STRUCTURE OF THESIS

The thesis is organized into five chapters. The first chapter gives an introduction to the impact of semiconductor research over the years, classification of semiconductors and how new semiconductor materials including ternary and quaternary alloys are being developed and used. The chapter also states the specific research objectives and finally describes how the thesis is structured.

The second chapter deals with review of literature on group II-VI semiconductor alloys. Emphasis is placed on the optical and transport properties of $\text{Cd}_{1-x}\text{Zn}_x\text{S}$ ternary alloy deposited with different methods under different conditions. The third chapter treats the relevant theory.

Methodology and materials used in doing this research are presented in the fourth chapter, while the fifth chapter deals with results in graphical format and in-depth discussion of results. In the sixth chapter conclusions and recommendations are made. Lastly, references cited in this thesis and appendices are presented.

CHAPTER TWO

2. LITERATURE REVIEW

2.0. SEMICONDUCTOR ALLOYS

An alloy is a combination, either in solution or compound, of two or more elements. The resulting alloy substance generally has properties significantly different from those of its components. An alloy with two components is called a binary alloy. Semiconductor alloys can be formed in various ways. Binary alloys are made by mixing similar elements such as Si and Ge, for example, to form $\text{Ge}_x\text{Si}_{1-x}$. Ternary alloy is an alloy made up of three different chemical elements; usually two cations and an anion. Ternary alloys of compound semiconductors can be obtained by substituting an element such as Al for the homologous element Ga in GaAs to form $\text{Ga}_{1-x}\text{Al}_x\text{As}$. Alternatively, one can mix the non metal constituents by substituting S for Se in ZnSe to give $\text{ZnS}_x\text{Se}_{1-x}$. Quaternary alloys results if both the metal and nonmetal constituents are mixed to give, for example, $\text{Ga}_x\text{Al}_{1-x}\text{P}_y\text{As}_{1-y}$. The band gap of an alloy is a continuous function of composition. In ternary alloys, the variation with composition is linear if the two constituents that are varied have nearly the same atomic radii and the same bonding strength to the third constituent (Adachi, S., 2009; Balkanski, M. and Wallis, R.F., 2000).

2.1. WHY THE INTEREST IN $\text{Cd}_{1-x}\text{Zn}_x\text{S}$

In recent years, extensive studies have been carried out on the preparation and characterization of wide band gap oxide semiconductors such as TiO_2 , ZnO, SnO_2 (Minami, T. *et al.*, 2006), etc. due to their application in photovoltaic, photo

electrochemical energy conversion and photoconductors. The cadmium zinc sulphide (Cd, Zn)S ternary alloy is one of the promising materials in this respect (Kumar, V. *et al.*, 1998). Interest in (Cd, Zn)S has been driven by the expected improvement in performance of thin film photovoltaic cells of type CdTe- and CIS(CuInSe₂-based cells) using (Cd, Zn)S rather than the presently used CdS. This expectation arises mainly from the increased band gap of the Zn-containing solid solution, resulting in increased transparency to shorter wavelength of light. Another consideration for heterojunction formation is the decrease in electron affinity of the semiconductor with increase in Zn content (ZnS has a smaller electron affinity than CdS). The electron affinity of a semiconductor is a measure of the position of the conduction band with respect to the vacuum energy level; a lower value means a higher conduction band. Thus the alignment of the conduction band of the (Cd, Zn)S with that of the second semiconductor can be controlled to a large extent by varying the film composition (Hodes, G., 2002).

2.2. ELECTRICAL, OPTICAL AND STRUCTURAL CHARACTERIZATION **OF Cd_{1-x}Zn_xS**

Cd_{1-x}Zn_xS ternary compounds can form a continuous series of solid solution allowing systematic variation of the band gap from 2.43 eV for CdS to 3.7 eV for ZnS by adjusting the composition (Yokogawa, T., *et al.*, 1994). In CdS/CdTe solar cells, the replacement of CdS with the higher band gap ternary (Cd, Zn)S film can lead to a decrease in window absorption losses, and has resulted in an increase in the short-circuit current (Yamaguchi, T. *et al.*, 1996).

In spite of the overall chemical similarity of Cd and Zn, however, it has not proven simple to deposit true solid solution of the sulphides. One point in favour of a single-phase solid solution deposition is that CdS and ZnS do readily form solid solution in general. Thus, if the two sulphides can be simultaneously deposited, there is a good chance that they will form a solid solution if the temperature is high enough. Put another way, annealing of a well-mixed two-phase mixture of CdS and ZnS will form a solid solution if the temperature is high enough (Hodes, G., 2002).

The (Cd, Zn)S has been prepared by various methods such as vacuum evaporating, screen printing, sintering, chemical deposition, physical vapour deposition, spray pyrolysis, dip technique, electrodeposition etc. Among these, the dip technique is cheaper, relatively simpler and more versatile than the others and gives the possibility of obtaining films with suitable properties for optoelectronic applications and also when large area deposition is needed (Karanjai, M.K. and Dasgupta, D., 1986).

The dip technique as used for the preparation of sulphide films is a modification of the well known spray pyrolysis method. In the latter technique the reactants impinge on a preheated substrate where the film-forming chemical reaction takes place. In contrast to spray pyrolysis, the dip technique allows the reactants and the substrate to rise in temperature at the same rate. CdS films formed by the two techniques are very similar. However, for ZnS and $\text{Cd}_{0.8}\text{Zn}_{0.2}\text{S}$ films, there are significant differences (Karanjai, M.K. and Dasgupta, D., 1986).

The dip technique for the preparation of oxide thin films was quite popular before the widespread use of the vacuum evaporation technique. At first, this method was limited to oxide films only. The method involves the dipping of the substrate in a solution of the corresponding metal nitrate in an organic solvent, withdrawal at a

controlled speed and subsequent high temperature baking where the nitrate decomposes to yield the oxide. It has been found that, by adding a suitable sulphur containing compound like thiourea, sulphide films can also be deposited by this technique (Karanjai, M.K. and Dasgupta, D., 1986; Schroeder, H., 1969). In the present work cadmium nitrate, zinc nitrate and thiourea were used and upon high temperature baking cadmium- zinc- sulphide was formed, with all the other products escaping as volatile compounds.

Karanjai, M. K. and Dasgupta, D., 1986, used the dip technique in the preparation of sulphide thin films on soda-glass substrates, including Cd, Zn and Cd-Zn mixed sulphide films. The films were reported to be uniform except for a vertical region about 2 mm wide (in the orientation in which the substrate was withdrawn) on the sides of the substrate and a horizontal region about 1cm wide at the bottom of the substrate. The thicker layer at the sides was as a result of edge non-uniformity and that at the bottom was produced because an extra amount of liquid adhered there after dipping, owing to surface tension. The characterization of the films was, however, performed on the uniform central portions of the films. By varying the ion concentration in the starting solution a range of thicknesses of about 500-5000 Å could be obtained per dipping. Smooth films were obtained at low thicknesses (not more than 3000 Å) but films were rough and grainy at higher thicknesses (about 10000 Å). The gravimetric method was used in estimating the thickness of the rough films, because standard optical interferometric techniques could not be used.

Adhesion of CdS films to the substrate was found to be dependent on the Cd:S ratio in the starting solution. Films with Cd:S = 2:1 and 1:1 were strongly adherent; a

behaviour attributed to the formation of a certain amount of CdO, which bonds strongly with the substrate surface, whereas those with Cd:S = 1:2 had very poor adhesion properties. ZnS and Cd_{0.8}Zn_{0.2}S films with M:S = 1:1 also showed good adhesion. The surface morphology of the CdS films indicated that the grain size does not depend significantly on the baking temperature. It was, however, found that the grain size increases rapidly with the number of dippings but levels off after about five to six dippings. Except for the film produced by a single dipping, all subsequent films are really deposited on the underlying CdS layer and it is clear that this exerts a substantial influence on the growth of the subsequent layer formed. This is also corroborated by the fact that the rate of increase in thickness per dipping is lower for the first dipping compared with the subsequent dippings (Karanjai, M.K. and Dasgupta, D., 1986).

It was also found that the smoothness of the films, as can be observed visually increases with the number of dippings, this is probably in connection with the increase in grain size already mentioned. Films produced by more than five dippings showed evidence of dendrite-like growth (Karanjai, M.K. and Dasgupta, D., 1986).

X-ray diffractograms for typical films with Cd:S ratios of 1:1, 2:1 and 1:2 showed a predominantly zinc blende structure. In addition, films with a Cd:S ratio of 2:1 showed peaks corresponding to CdO as may be expected. The films with 1:1 stoichiometry gave the best diffraction peaks.

From optical transmission measurements the absorption edge occurred at approximately 520 nm, corresponding to a band gap of 2.38 eV. Zelaya-Angel *et al.*, 1995, reported energy band gap decrease of CdS from 2.43 to 2.25 eV as the annealing temperature increased from 100 to 250 °C. The band gap was minimum for annealing

temperature of about 300 °C and afterwards increased to 2.35 eV at an annealing temperature of 400 °C.

The ZnS films indicated a grainy structure essentially similar to those of CdS. X-ray diffractometry showed, however, that the films were completely amorphous with absorption edge occurring at approximately 340 nm, that is, a band gap of about 3.64 eV (Karanjai, M.K. and Dasgupta, D., 1986).

The Cd-Zn mixed sulphide films consisted of an aggregate of amorphous zinc sulphide and partially crystalline CdS phases. The grain size, typically 1 µm, was found to increase with number of dippings.

The structural, electronic and optical properties of $Cd_{1-x}Zn_xS$ ($0.0 \leq x \leq 0.6$) thin films prepared by the spray pyrolysis technique have also been investigated by Oztas and Bedir. The deposited films were reported to be single phase in nature because of the Vegard-like variations in lattice size. Their $Cd_{1-x}Zn_xS$ films were visibly inferior to the CdS films because of increased roughness and presence of gross microstructural non-uniformities.

The electrical and optical properties of the Zn-containing films were similar to those of CdS thin films except that the mobility was much lower. The mobility decreased to very low values when the Zn concentration was comparable to that of Cd. It was also observed that as Zn lowered the film mobility, it increased the carrier density slightly. Films doped with In exhibited higher mobilities and carrier densities, however, increasing Zn content still decreased the mobility. Grain size was also observed to increase with In doping. Chemisorbed oxygen is known to affect the transport properties of II-IV compound films primarily through either serving as a compensating acceptor in

n-type films or as an electron trap at grain boundaries. It was found that the higher Zn content appeared to accentuate the detrimental effects of chemisorbed oxygen. One possibility is that the grain size of the films decreased with increasing Zn. The corresponding increase in grain boundary surface area and increased chemisorbed oxygen in addition to the smaller grains may be responsible for the observed decrease in film mobility with increasing Zn (Oztas, M. and Bedir, M., 2001).

Song *et al.*, 2005, studied (Cd, Zn)S thin films grown on the soda-lime glass substrates by chemical bath deposition technique (CBD) process for buffer layer applications in CuGaSe₂ (CGS) solar cells. The structural, surface morphology, optical and electrical properties of the as deposited films were investigated by XRD, SEM, spectrophotometer and four probes resistivity measurements as a function of Zn-composition in the solution. The films had hexagonal structures and the grain size increased with increasing Zn- content in the solution. The resistivity of the CdZnS films were reported to increase as the Zn content increased.

Optical absorbance (A) and transmittance (T) spectra of the films were measured using an HP 8453 UV-Visible spectrophotometer over the wavelength range of 300 to 1100 nm. The film with 30% of Zn in the solution showed a better than 80% transmittance for wavelengths longer than 600 nm and film thickness less than 50nm. The values of energy band gaps obtained were 2.40, 2.55 and 2.70 eV for Zn- content of 0, 30 and 50%, respectively.

The first well-characterized deposition of a true (Cd, Zn)S alloy film prepared by chemical bath deposition was described by (Padam *et al.*, 1988). In their work Cd and Zn acetates were used in various ratios complexed with ammonia, TEA and thiourea at

90-95 °C to deposit (Cd, Zn)S over the complete composition range onto glass substrates. Interestingly, the Zn was more heavily complexed than the Cd in this solution, which shows that the mechanism of deposition is not one based solely on solubility product of the sulphides. In fact, from the crystal size measurement of a similar deposition described by (Al Kuhaimi, S.A. and Tulbah, Z., 2000), it is possible that the deposition mechanism is different for the two cations. The small crystals of pure ZnS and the larger ones of pure CdS suggest a cluster mechanism and an ion-by-ion mechanism, respectively.

The films were characterized by a variety of techniques. Elemental analysis using electron diffraction (ED) showed that the Zn:Cd ratio in the film was almost equal. X-ray diffraction (XRD) and ED were used for phase and compositional analyses. All the compositions up to 80% Zn were wurtzite structure, while pure ZnS was sphalerite. Interestingly, while most of the films gave ring ED patterns showing nonoriented growth, some showed a degree of orientation, in spite of the glass substrate.

The band gap, calculated from optical absorption spectroscopy, varied almost linearly with composition between that of CdS (2.4 eV) and ZnS (3.6 eV). It is worth noting here that the band gap can differ slightly depending on the method employed for film deposition.

The films were all n-type (hot probe) with resistivity ρ that varied linearly on a log ρ scale from 10^9 Ω -cm (CdS) to 10^{12} Ω -cm (ZnS). Doping by In (as InCl_3 in the deposition solution) reduced ρ ; e.g., for a $\text{Cd}_{0.8}\text{Zn}_{0.2}\text{S}$ film, ρ dropped linearly on a log ρ scale with In content from ca. 10^{10} Ω -cm (undoped) to ca. 10^5 Ω -cm (1.5% In—the In ratio in the film was similar to that in the solution). At high In ratios, ρ increased,

explained by a decrease in mobility due to scattering by In. Annealing in H₂ at 200°C also decreased ρ . For example, a Cd_{0.8}Zn_{0.2}S: 1.5% In film showed a minimum value for ρ of ca. 10 Ω -cm, presumably due to loss of S.

This same method was more recently repeated with very similar results by (Al Kuhaimi, S.A. and Tulbah, Z., 2000). It was additionally found that the films were strongly textured, with only one XRD peak—either (001) wurtzite or (111) sphalerite, although this texture was lost if a subsequent layer was deposited to produce thicker films. The crystal size measured from XRD peak width varied from 20 nm (CdS) to 9 nm (ZnS). The band gap varied between the same limits as found in the previous study, but changed more rapidly for high Zn content. The resistivity of the films varied linearly on a log ρ scale from 10⁹ Ω -cm (CdS) to 10¹⁴ Ω -cm (ZnS)—the latter higher than the value measured by Padam *et al.*, 1988, as evidenced in figure 2.1. Boron doping decreased the resistivity of CdS by three orders of magnitude.

Using ammonia-complexed metal iodide and thiourea at pH 10, (Yamaguchi, T. *et al.*, 1996) have formed films whose properties depended on the temperature of deposition. The resistivity of the films decreased with increase in Zn content from 10¹⁰ Ω -cm for CdS (a very high value for CdS) to ca. 10⁶ Ω -cm for 90% (solution concentration) Zn and then increased to ca. 10⁹ Ω -cm for pure ZnS. No explanation for this effect was given. The films were photoconductive, with the resistivity decreasing in a somewhat sporadic manner as a function of composition, up to a maximum dark: light ratio of 5x 10³ for the 90% Zn films.

Similar conditions, but at a lower pH of 8.4, were also used by the group (Yamaguchi, T. *et al.*, 1999) in film deposition. X-ray diffraction showed well-defined

peaks that shifted in position with change in composition, while the optical absorption spectra gave values of E_g that also varied gradually with composition.

The well-defined shift in XRD peaks and, to a somewhat lesser extent, the gradual change in estimated band gap with composition provide good evidence for true solid solution formation.

Unlike other studies as well as the higher pH studies by the same group, the electrical resistivity did not vary much with composition, being ca. $5 \times 10^7 \Omega\text{-cm}$. An overview of the variation of resistivity of some of these (Cd, Zn)S films with composition is given in figure 2.1. There is quite a large variation, both in resistivity values and in their compositional dependence.

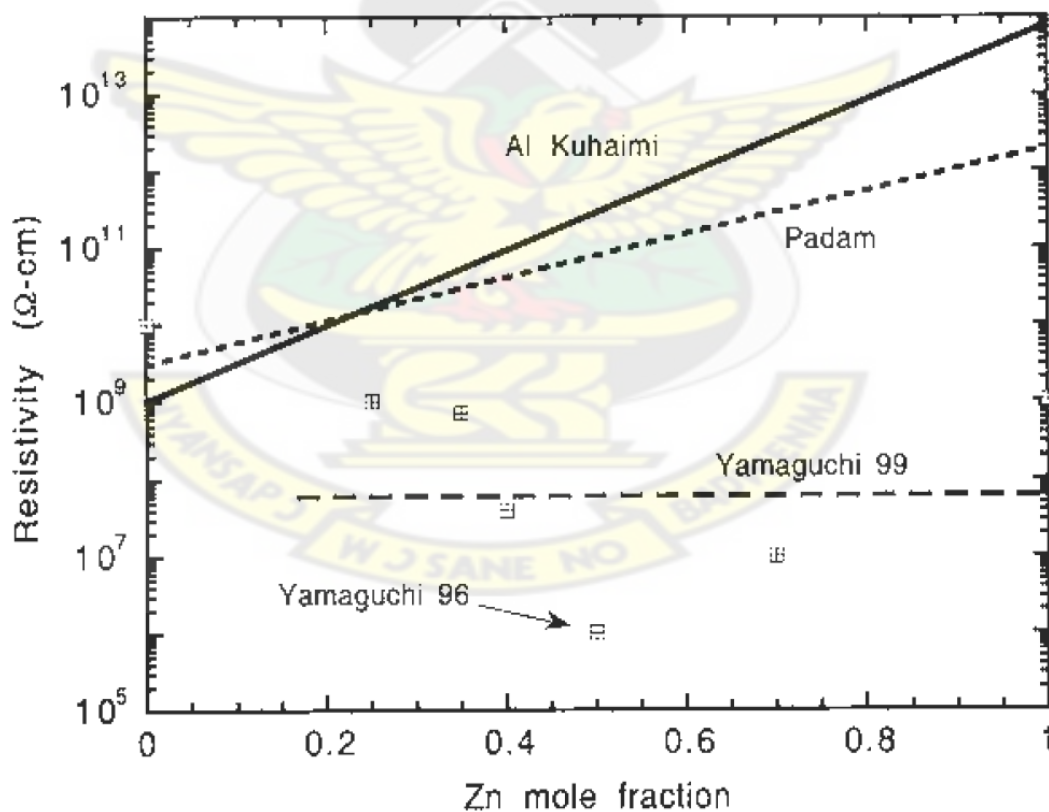


Figure 2.1. Resistivity data for some (Cd,Zn)S films. The data from the two Yamaguchi papers were modified to show resistivity values as a function of approximate film composition, rather than solution composition as given in the original papers.

The structural, composition and optical absorption properties of $\text{Cd}_{1-x}\text{Zn}_x\text{S}$ (CdZnS) thin films fabricated by the reactive diffusion of Zn in CdS have been investigated by (Dzhafarov *et al.*, 2006). This followed an earlier successful interdiffusion of Zn into CdTe by the same group. CdS thin films of 0.6-4.5 μm thickness were first deposited onto glass substrates by the close-spaced sublimation (CSS) technique. Chemical and mechanical polishing was performed on the surface of the CdS films before the Zn evaporation. Zn/CdS structures were formed by electron-beam evaporation of Zn films of 80-275 nm thickness on the CdS surface at room temperature.

The films were characterized by XRD, energy dispersive x-ray fluorescence (EDXRF) and optical absorption measurements. It was established that thermal annealing of Zn/CdS structure at temperature (400 °C) lower than the melting point of Zn (418 °C) results in the concentration distribution of Zn in CdS film described by an erfc-curve ($D = 5 \times 10^{-14} \text{ cm}^2\text{s}^{-1}$) and characterizing the free impurity diffusion from a constant source. In contrast to this, the concentration profile of Zn in CdS film at higher annealing temperature (570 °C) is not described by the erfc-curve and shows a nearly stepped form, which is characteristic of reactive diffusion. The XRD patterns of the CdS film show the peaks are characteristic of hexagonal CdS. XRD patterns of Zn/CdS structures exposed to heat annealing at 570 °C 6 minutes are shown in figure 2.2.; the diffraction peaks indicate the presence of ternary CdZnS compounds. The patterns were similar to those for the CdS with small displacement of all peak positions to larger 2θ . For comparison, figure 2.2.(c) illustrates the clear displacement of the (101) peak

position of Zn/CdS ($2\theta=28.4748^\circ$) compared with the (101) CdS peak ($2\theta=28.1939^\circ$). Interestingly, the XRD pattern for the Zn/CdS structure annealed at 400°C almost coincides with that for CdS annealed at the same temperature with about 0.004° difference in displacement of peak positions (Dzhafarov, T.D., *et al.*, 2006).

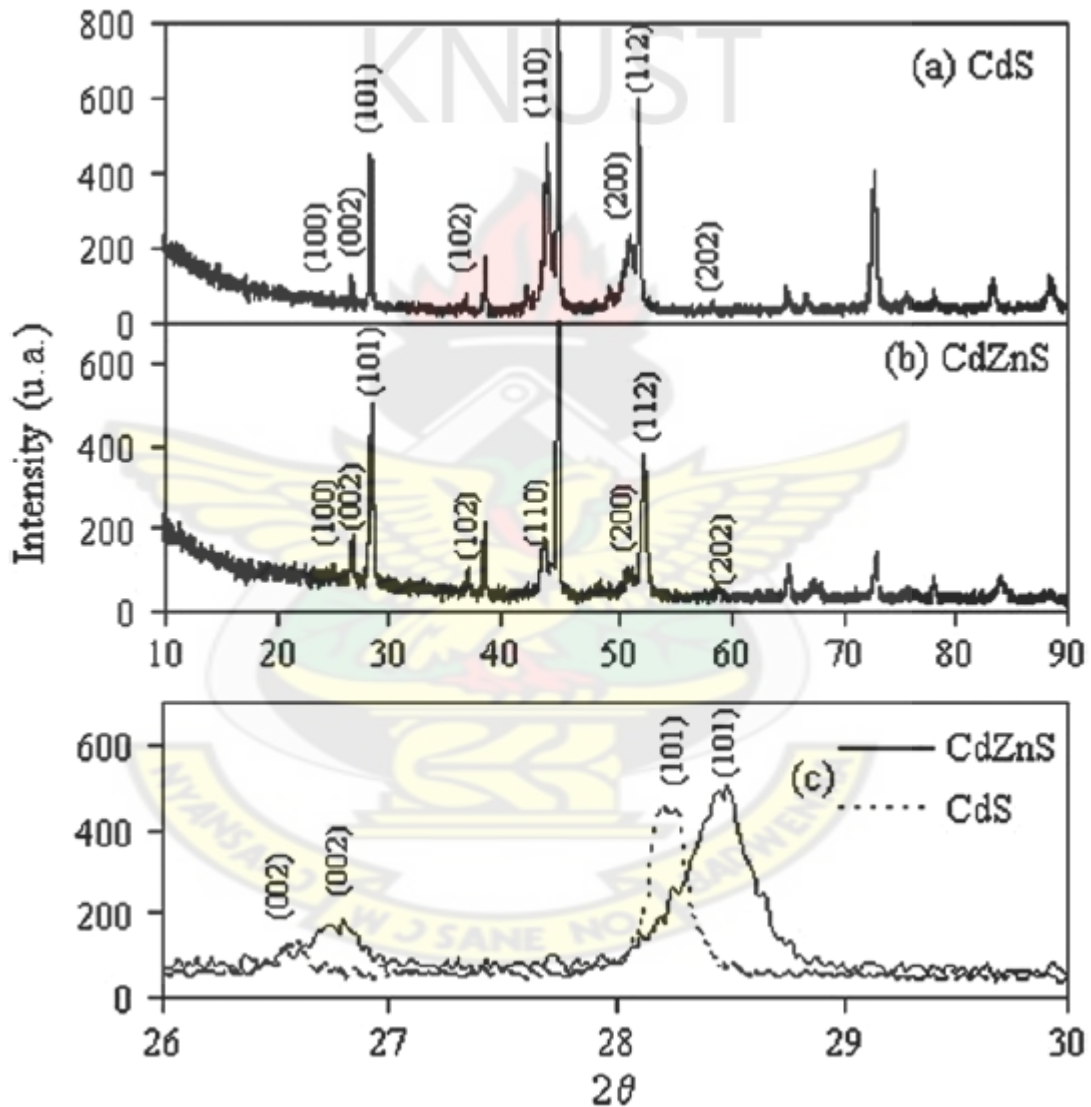


Figure 2.2. XRD patterns of (a) CdS, (b) Zn/CdS structure ($d_{\text{Zn}} = 275 \text{ nm}$, $d_{\text{CdS}} = 2 \mu\text{m}$) exposed to thermal annealing at 570°C for 5 min; (c) fragment of (a) and (b) patterns for $2\theta = 26\text{--}30^\circ$.

Analysis of the absorption spectrum of such films indicates formation of CdZnS compound with the largest value of energy band gap up to 2.64 eV, exceeding the band gap of CdS (2.43 eV). The spectrum of CdS film showed allowed direct band gap with single slope, while the spectrum of the Zn/CdS could not be characterized by one slope, but rather presents a curve with changing slopes.

Extrapolation of the linear portions of the high-energy and middle-energy regions of the curve to the energy axis gave 2.55 eV and 2.43 eV, respectively. Such behaviour of the Zn/CdS sample annealed at 570 °C can be caused by non-uniformity of the sample.

The XRD data of figure 2.2 confirms the above supposition. Thus the interdiffusion in Zn/CdS structures at temperatures exceeding the melting point of Zn was accompanied by the formation of $\text{Cd}_{1-x}\text{Zn}_x\text{S}$ ternary compounds (Dzhafarov, T.D., *et al.*, 2006).

2.3. LOW DIMENSIONAL $\text{Cd}_{1-x}\text{Zn}_x\text{S}$

Recent developments related to nanoengineered materials have demonstrated that nanostructure (with typical sizes in the range between about 1 and 50 nm) semiconductors offer increasingly greater flexibility and control in designing various nanoscale structures and devices. In this context, the main motivation is related to continuous trends towards increasing miniaturization of various structures and devices, improving dimensional precision and the high flexibility of controlling and designing various material properties by controlling the sizes of the nanostructures. Such nanostructures exhibit structural, optical and electronic properties that are unique to them and they are different from both macroscopic materials and isolated molecules

(Yacobi, B.G., 2004). It has been possible to deposit $\text{Cd}_{1-x}\text{Zn}_x\text{S}$ thin films on the nanoscale too.

Nanoparticles of $\text{Cd}_{1-x}\text{Zn}_x\text{S}$ with different compositions ($0 \leq x \leq 1$) embedded in silica matrix were prepared in thin film form by the sol-gel technique (Bhattacharjee *et al.*, 2002). The film texture and structural transformation with increasing x value were studied from transmission electron micrographs and electron diffraction patterns. The electron diffraction patterns of the films showed central halos with concentric ring patterns. The ring patterns indicated random orientation without any preferential directions. The rings became broader and fainter with increasing x apparently due to the reduction in crystallite sizes with higher Zn content. The diffraction pattern of the CdS film ($x = 0$) showed hexagonal structure as already reported but in this case with reflections from (002) and (110) planes. For the ZnS film ($x = 1$), prepared under identical conditions, the rings were too broad and faint and the reflecting planes could not be identified. However, when this ZnS film was annealed at a higher temperature ($\sim 573\text{K}$) well crystallized film texture could be observed with particle radius ~ 3.5 nm. The corresponding diffraction pattern showed sharp rings due to (111), (220) and (200) planes of a cubic structure (Bhattacharjee *et al.*, 2002). The change in crystal structure from hexagonal CdS to cubic ZnS with increasing Zn is well established (Padam *et al.*, 1988).

Figure 2.3 shows the variation of absorption coefficient (α) with photon energy ($h\nu$) for films with different Zn contents. The absorption edge shifted to higher energy with increasing Zn content due to two superimposed effects. Increase in band gap in the solid solution of (Cd, Zn)S for higher Zn is a bulk property. On the other hand, as x

increases particle size decreases, resulting in higher band gap due to increasing contribution of quantum size effect (Bhattacharjee *et al.*, 2002).

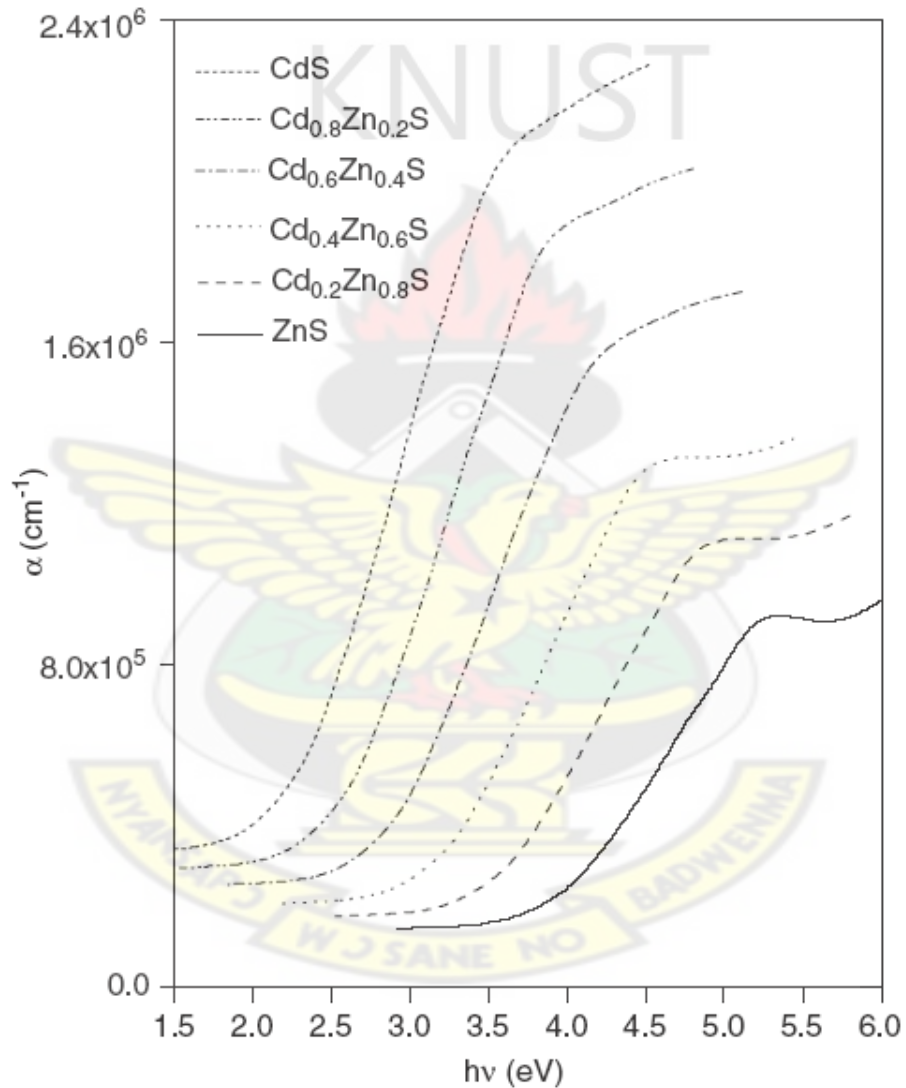


Figure 2.3. Variation of optical absorption coefficient (α) with photon energy ($h\nu$) for different compositions (x value) of $\text{Cd}_{1-x}\text{Zn}_x\text{S}$ films.

Thus in studying the optical properties of ternary nanocrystalline semiconductor films like $\text{Cd}_{1-x}\text{Zn}_x\text{S}$ the size dependence should be considered in addition to the compositional variation. For a fixed composition or x value, post deposition annealing time and temperature may be chosen carefully to obtain particle size as desired and this may provide a convenient way to fine tune the properties of nanocrystalline semiconductors for practical application.

Optical studies indicated increase in optical band gap (see figure 2.4) and decrease in refractive index with increasing zinc content (x value). Photoluminescence studies showed emission from surface states with emission energy blue shifted with increasing zinc content in the films (Bhattacharjee *et al.*, 2002).

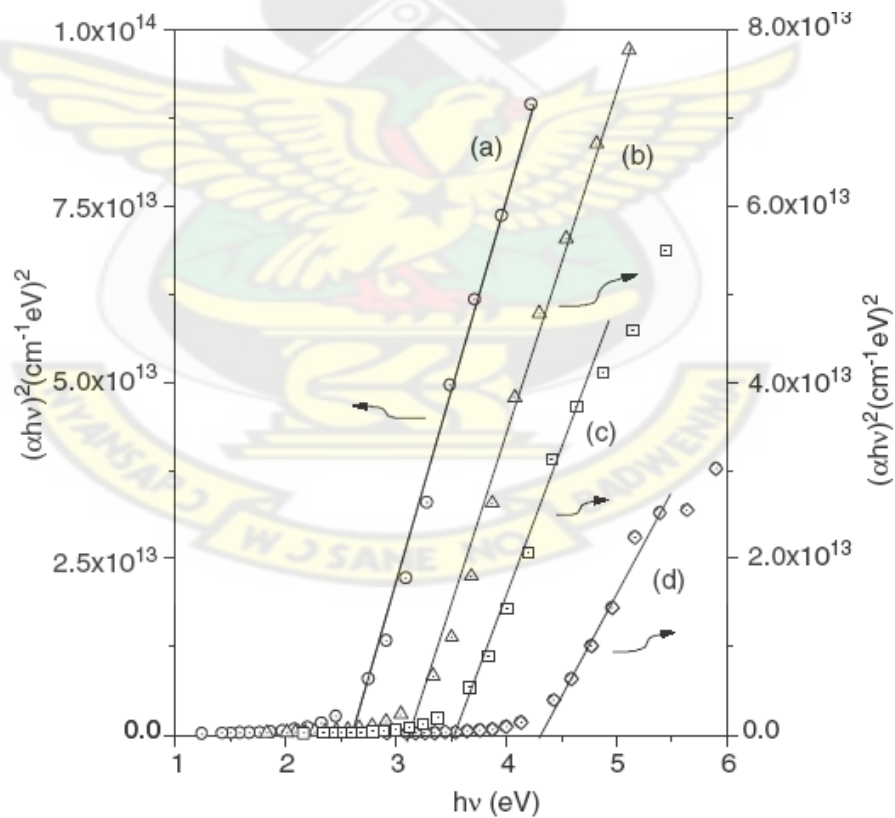


Figure 2.4. Plot of $(\alpha h\nu)^2$ vs $h\nu$ for four different compositions: (a) $x = 0$, (b) $x = 0.4$, (c) $x = 0.6$ and (d) $x = 1$.

2.4. BASICS OF FILM FORMATION AND STRUCTURE

Thin film technology is simultaneously one of the oldest arts and one of the newest sciences. Involvement with thin films dates to the metal ages of antiquity. As a modern science, thin films have been prepared ever since vacuum systems first became available, but deposition as a means of producing films for device purposes is a development of the past 40 years. Thin metallic film coatings on glass or plastic were among the first to be exploited for optical purposes, ranging from mirrors to sunglasses, and this still continues as a major, typically high vacuum, high throughput business. As thin film deposition processes have developed very rapidly over the past 25 years, particularly in the context of semiconductor devices, processes have become highly specialized (Ohring, M., 1992; Venables, J.A., 2003).

Films can be grown by various methods: deposition of material from vapour, liquid (melt or solution) and solid phases; deposition from molecular and ionic beams; by thermal or ionic scattering; with the help of chemical reactions at the substrate surface (oxidation, anodization, nitriding, formation of silicides, etc.), and by electrolytic methods (Poole, C.P.Jr., 2004).

Sulphide thin films find extensive use in the fabrication of a number of solid state devices such as photoconductors and solar cells, thin film transistors and electroluminescent cells. A large variety of deposition techniques which include vacuum evaporation, spray pyrolysis, sputtering, molecular beam epitaxy (MBE), vapour phase epitaxy, chemical vapour deposition (CVD), solution growth, screen printing and electrophoresis have been used for the preparation of these films (Chopra, K.I. and Kaur, I., 1983). In this work the relatively simple and low cost dip technique has been used.

All phase transformations, including thin film formation, involve the processes of nucleation and growth.

Film growth, by whatever technique is used, can typically be described in terms of three main events: (1) nucleation, (2) crystal growth, and (3) grain growth. *Nucleation* is the process of the vapour-phase atoms or molecules coming together to form a condensed unit. Soon after exposure to the substrate to the incident vapour, a uniform distribution of small but highly mobile clusters or islands is observed. The next stage involves merging of the islands by a coalescence phenomenon that is liquid like in character especially at high substrate temperatures. Crystallographic facets and orientations are frequently preserved on islands and at interfaces between initially disoriented, coalesced particles. Coalescence continues until a connected network with unfilled channels in between develops. With further deposition, the channels fill in and shrink, leaving isolated voids behind. Finally, even the voids fill in completely, and the film is said to be continuous. This collective set of events occurs during the early stages of deposition, typically accounting for the first few hundred angstroms of film thickness.

The many observations of films formation have pointed to three basic growth modes: (1) island (or Volmer-Weber), (2) layer (or Frank-van der Merwe) and (3) Stranski-Krastanov, which are illustrated schematically in figure 2.5.

Island growth occurs when the smallest stable clusters nucleate on the substrate and grow in three dimensions to form islands. This happens when atoms or molecules in the deposit are more strongly bound to each other than to the substrate. The opposite characteristics are displayed during layer growth. Here the extension of the smallest stable nucleus occurs overwhelmingly in two dimensions resulting in the formation of planar sheets. The assumption is that the adsorbed atoms have a stronger attraction for

the substrate than they do for one another, which is why each layer is completed before the next layer is started (Ohring, M., 1992; Lalena, J.N., *et al.*, 2008).

The layer plus island or Stranski-Krastanov growth mechanism is an intermediate combination of the aforementioned modes. In this case, after forming one or more monolayers, subsequent layer growth becomes unfavorable and islands form. The transition from two- to three-dimensional growth is not completely understood, but any factor that disturbs the monotonic decrease in binding energy characteristic of layer growth (e.g., lattice mismatch and strain energy) may be the cause.

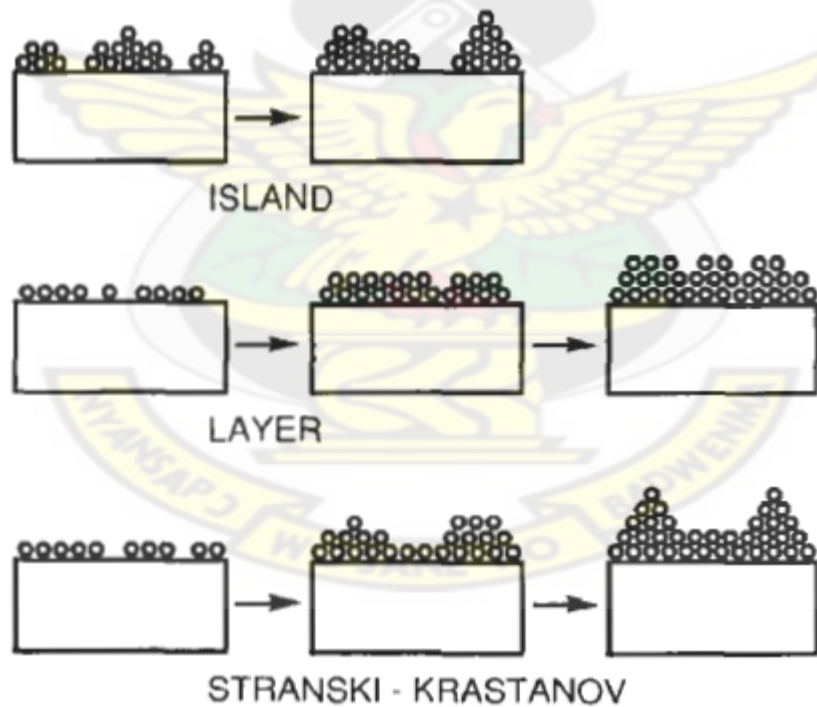


Figure 2.5. Basic modes of thin film growth.

When film is deposited “slowly,” there are grains, vacancies and stacking faults present. Films deposited at “high” rate have grain structure that is considerably finer and more disordered with numerous point defects, voids and grain boundaries present. When the rapidly deposited films are annealed through a magnetic vibrator, vacancies are annihilated, faults are eliminated and grains reorient, coalesce and grow. A larger grain means a return to the spotted diffraction pattern (Ohring, M., 1992).

For “concentrated” alloys containing equal numbers of large and small spheres with a size difference of 27%, the as-deposited structure is amorphous. Upon vibration annealing, the film become dense slightly, but the atomic logjam cannot be broken up. There is no appreciable change in its structure- it is still amorphous. For less concentrated alloys (~ 17%), however, the as-deposited structure is very fine grained but apparently crystalline.

All of the foregoing results were for films deposited on the smooth substrate. The “crystalline substrate” affords the opportunity to model epitaxy phenomena. Pure films deposit in almost perfect alignment with the substrate when deposited slowly. Imperfect regions are readily eliminated upon annealing and nearly perfect singly crystals are obtained. Rapidly deposited films are less influenced by the underlying substrate and remain polycrystalline after annealing. Clearly epitaxial growth is favoured by low deposition rates. The presence of alloying elements impeded epitaxy from occurring in accord with experience (Ohring, M., 1992).

2.5. ANNEALING

Annealing is heat treatment of materials at elevated temperatures aimed at investigating or improving their properties. Material annealing can lead to phase

transitions, recrystallization, polygonization, homogenization, relaxation of internal stresses, removal of aftereffects of cold plastic deformation (strain hardening), annihilation and rearrangement of defects and so on. The results of annealing depend significantly on its kinetics: the rate of heating and cooling and the time of exposure at a given temperature.

2.5.1. IRRADIATION ANNEALING

This is the annealing of defects in a crystal stimulated by nuclear radiations. Both impurity atoms and other defects formed prior to irradiation, as well as radiation-induced defects take part in the process. When radiation doses are large, annealing lowers the rate of accumulation of the defects, particularly if the intensities are high enough. Irradiation annealing mechanisms are related to the processes of radiation-induced diffusion of defects, to atomic restructuring triggered by collisions of external particles with crystal atoms and also the small dose effect (Poole, C.P.Jr., 2004).

2.5.2. RECRYSTALLIZATION ANNEALING

Heating a solid to a temperature that provides full recrystallization within a given time period. Recrystallization annealing is used to lower the dislocation density, to change texture, to form a polycrystal structure and thereby to bring the physical and chemical properties of a solid to a level characteristic of an unhardened annealed state. Conditions for this annealing of deformed materials are chosen using recrystallization diagrams which provide the dependences of the temperatures for the beginning and end of the initial recrystallization on the degree of strain for a given processing duration.

2.5.3. PULSED ANNEALING OF SEMICONDUCTORS

This is a high temperature treatment of semiconductor specimens which is characterized by sharp fronts of heating τ_h and cooling τ_c , in practice without holding the temperature at the maximum value. Values of τ_h and τ_c vary over a wide range. As a rule, they are set by the conditions of conserving the bulk properties, without noticeable diffusion of impurities, and this provides the possibility of fusing surface layers while conserving the crystal structure of the bulk. The process duration is from 10^{-12} s to several seconds. For pulses shorter than a few microseconds the most efficient results are achieved with exciting pulse energies sufficient for melting the surface layer. For longer pulses the target heating is almost uniform due to thermal conductivity. Particularly important results were obtained by combining pulsed annealing with ion implantation of impurities. The nonequilibrium introduction of impurities together with nonequilibrium annealing is the most efficient technique for obtaining highly doped, structurally perfect semiconducting layers. The pulsed annealing method is widely used for the restoration of a crystal structure disturbed during ion bombardment (Poole, C.P.Jr., 2004).

CHAPTER THREE

3. THEORITICAL BACKGROUND

3.0. CLASSIFICATION OF SOLIDS

There are diverse ways of classifying solids, but perhaps the most useful division is into *crystalline*, *polycrystalline* and *amorphous*. Each type is characterized by the size of an ordered region within the material. An ordered region is spatial volume in which atoms or molecules have a regular geometric arrangement or periodicity. Figure 3.1 shows the three structural orders (Neamen, D.A., 2003). It should be noted that the majority of semiconductors used in electronic applications are crystalline materials, although some polycrystalline and amorphous semiconductors have found a wide range of applications in various electronic devices, (Yacobi, B.G., 2004).

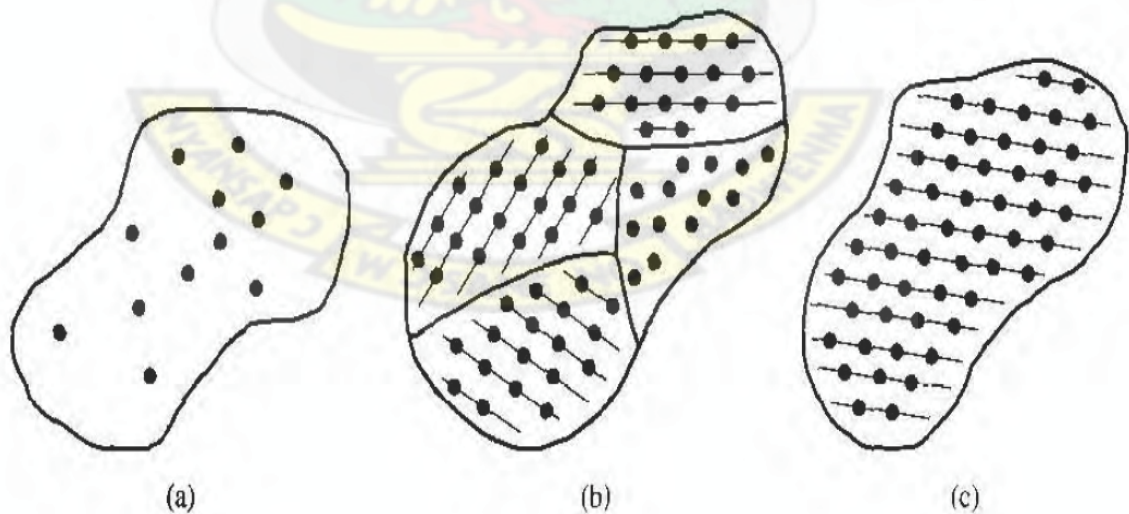


Figure 3.1. Schematics of the three general types of structural orders: (a) amorphous, (b) polycrystalline, (c) crystalline.

3.0.1. CRYSTALLINE SEMICONDUCTORS

In crystalline materials, the atoms are arranged in a periodic, regularly repeated three-dimensional pattern—thus presence of long-range order. The universe of traditional solid state physics is defined by the crystalline lattice. The principal actors are the elementary excitations like phonons, polarons, magnons etc in this lattice. Another is the electron that is perhaps the principle actor in all of solid state physics. By electron in a solid we mean something a little different from a free electron (Pettersen, J. D. and Bailey, B. C., 2005).

A. H. Wilson showed in 1931 how the electronic band theory of crystals developed by F. Bloch can be applied to the understanding of semiconductors. Properties such as the negative temperature coefficient of electrical resistivity follow naturally from Wilson's theory. The key ingredients are the *Bloch states* which are the eigenstates of an electron moving in the periodic potential of a crystal. The energies of the Bloch states cannot take on all possible values, but are restricted to certain allowed regions or *bands* separated from one another by forbidden regions called *band gaps* or *energy gaps*. Band theory and its outcome-effective mass theory-has allowed us to understand the difference between metals, insulators and semiconductors and how electrons respond to external forces in solids (Balkanski, M. and Wallis, R.F., 2000; Singh, J., 2003)

Information about the structure of solids can be obtained by plotting the so-called *radial distribution function*, which is the probability, $P(r)$, of finding an atom at a distance r from a given atom. In crystalline solids, such a radial distribution function exhibits series of sharp peaks indicative of the long-range order. The curve representing an amorphous material indicates the presence of the short-range order only. This also

implies that the number of nearest neighbors to any given atom, on average, is not much different from the corresponding number in the crystalline material.

The electronic band structure of crystalline semiconductors is substantially different from that in the amorphous semiconductors. In crystalline materials, the periodicity of the atomic structure and the presence of long-range order result in a band structure with allowed and forbidden electronic levels, with sharp band edges and a fundamental energy gap separating valence band from the conduction band. In amorphous semiconductors, there is still a fundamental energy gap based on the short-range bonding between the atoms; however, the sharp band edges of the crystalline semiconductor are replaced in the amorphous materials by *exponential band tails* due to localised states related to the structural disorder (i.e., bond length and bond angle deviations that broaden the distribution of electronic states); in addition, defects (i.e., dangling bonds) introduce electronic levels in the energy gap (Yacobi, B.G., 2004). From observations and measurements we find that it is the regular crystalline structure that leads to certain special properties and behaviour of the associated materials (Korvink, J.G. and Greiner, A., 2002). The advantage of crystalline material is that, in general, its electrical properties are superior to those of a nonsingle-crystal material, since grain boundaries tend to degrade the electrical characteristics (Neamen, D.A., 2003).

3.0.2. POLYCRYSTALLINE SEMICONDUCTORS

In polycrystalline materials, numerous crystalline regions called *grains*, have different orientation and are separated by a *grain boundary*. That is, they have a high degree of order over many atomic or molecular dimensions. These ordered regions or

single-crystal regions only vary in size and orientation with respect to one another (Neamen, D.A., 2003).

These semiconductors can be further classified as (i) microcrystalline and nanocrystalline materials that are usually prepared as thin films and (ii) large grain materials in the form of sliced ingots and sheets. The grain size in polycrystalline materials depends on the substrate temperature during thin film growth, the thickness of the film and also on post-growth annealing treatment of the film. It is important to consider here that many solids are incorrectly described as being amorphous, but are in fact microcrystalline or nanocrystalline with small crystallite sizes which fail to give crystalline X-ray diffraction patterns. However, often these materials can be confirmed as crystalline using electron diffractions, with lattice images routinely obtained from particles in the range of 5 nm. The grain boundaries generally have an associated space-charge region controlled by the defect structure of the material and the grain boundaries are paths for the rapid diffusion of impurities affecting various properties of polycrystalline materials. An important consequence of the presence of potential barriers on grain boundaries in a polycrystalline semiconductor is the increase of its electrical resistivity. One of the important processes is the decoration of grain boundaries, that is, the process in which precipitates of impurity elements segregate to the boundaries.

In general, the grain boundaries introduce allowed levels in the energy gap of a semiconductor and act as efficient recombination centers for the minority carriers. This effect is important in minority-carrier devices, such as photovoltaic solar cells and it is expected that some of the photogenerated carriers to be lost through recombination on the grain boundaries. Typically, the efficiency of the device will improve with increasing grain size. In this context, the *columnar grain structure* (i.e., grains in a

polycrystalline material extend across the wafer thickness) is more desirable as compared to the material containing fine grains that do not extend from back to front of a device structure. In order to prevent significant grain boundary recombination of the minority carriers, it is also desirable that the lateral grain sizes in the material be larger than the minority carrier diffusion length. It should also be mentioned that the possible preferential diffusion of dopants along the grain boundaries and or precipitates of impurity elements segregated at the boundaries may provide shunting paths for current flow across the device junction.

It should also be noted that hydrogen passivation of grain boundaries in polycrystalline silicon devices, such as photovoltaic cells, is an effective method of improving their photovoltaic performance efficiency. This improvement is associated with the mechanism similar to that of the passivation of dangling bonds in amorphous silicon (Yacobi, B.G., 2004; Gellings, P.J. and Bouwmeester, H. J. M., 1997)

3.0.3. AMORPHOUS SEMICONDUCTORS

In contrast to crystalline materials amorphous semiconductors have only short-range order with no periodic structure see figure 3.3. These materials can be relatively, inexpensively produced as thin films deposited on large area substrates (Yacobi, B.G., 2004). An interesting aspect of thin film deposition techniques is that they facilitate the formation of amorphous metal and semiconductor structures relative to bulk preparation methods (Ohring, M., 1992).

What happens to the electron energy band model in a solid without regular crystalline order? The Bloch theorem is not applicable when the structure is not periodic, so that the electron states cannot be described by well-defined k values. Thus, the

momentum selection rule for optical transitions is relaxed; hence all infrared and Raman modes contribute to the absorption spectra. The optical absorption edge is rather featureless. And since momentum conservation rules for direct and indirect optical transitions no longer apply, in the case of amorphous silicon, e.g., this results in very high absorption coefficient, allowing the use of only micrometer scale thin films for absorption of solar energy. As previously noted, allowed bands and energy gaps still occur because the form of the density of states (DOS) versus energy is determined most strongly by local electron bonding configurations.

In amorphous semiconductors, charge carriers may be scattered strongly by the disordered structure, so that the mean free path may sometimes be of the order of the scale of the disorder. Anderson, 1963, proposed that the states near the band edges may be localised and do not extend through the solid. It should be noted that the transition from the localised states to the extended states results in a sharp change in the carrier mobility, leading to the presence of the mobility edges or the mobility gap. The carrier mobility in the extended states is higher and the transport process is analogous to that in crystalline materials; whereas in the localised states, the mobility is due to thermally-activated tunneling between those states (i.e., *hopping conduction*) and it is lower as compared to the extended states. Thus, Anderson localization transition caused by random local field fluctuations due to disorder can lead to “mobility edges” rather than band edges as illustrated in figure 3.2 and hence, rather than an energy gap one has a mobility gap separating localised and nonlocalised or extended states (Kittel, C., 2005; Yacobi, B.G., 2004; Petterson, J. D. and Bailey, B. C., 2005)

Two distinct classes of amorphous semiconductors are widely studied: tetrahedrally-bonded amorphous solids such as silicon and germanium and chalcogenide

glasses. The latter are multicomponent solid of which one major constituent is a “chalcogen” element—sulphur, selenium, or tellurium (Kittel, C., 2005).

The tetrahedrally-bonded materials have properties similar to those of their crystalline forms, provided the dangling bonds defects are compensated with hydrogen. They can be doped with small amount of chemical impurities and their conductivity can be sharply modified by injection of free carriers from a metallic contact. By contrast, the chalcogenide glasses are largely insensitive to chemical impurities and to free carrier injection.

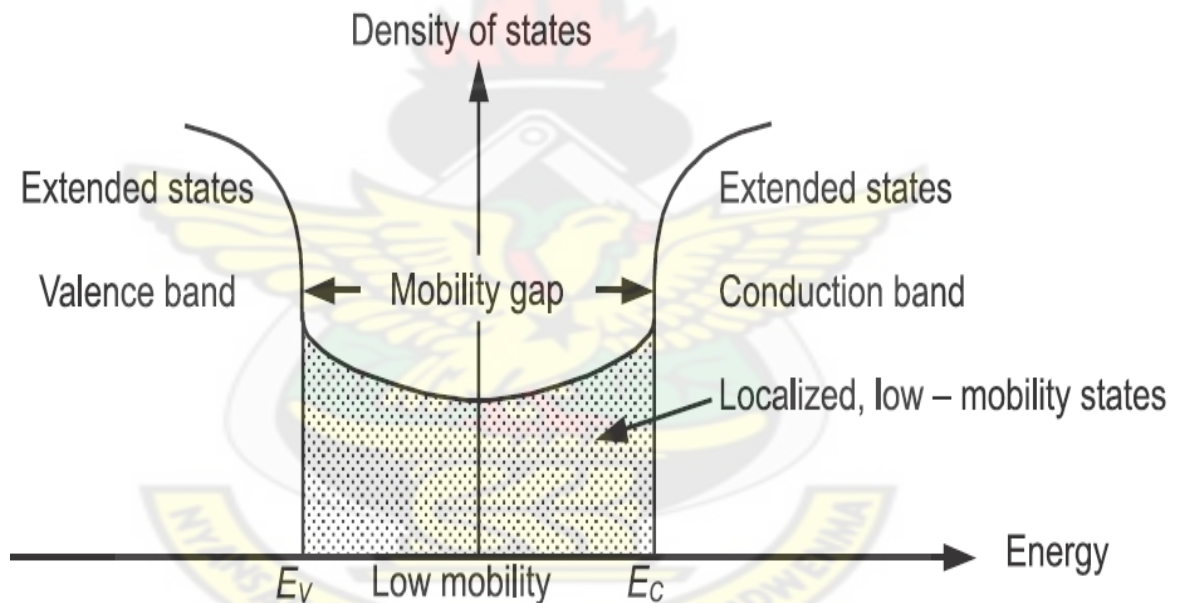


Figure 3.2. Area of mobility between valence and conduction bands

In amorphous materials, defects are of different kind as compared to crystalline materials. In the case of amorphous materials, the main defects are those related to the deviations from the average coordination number, bond length and bond angle; other

defects include, e.g., dangling bonds, deviations from an optimal bonding arrangement and microvoids.

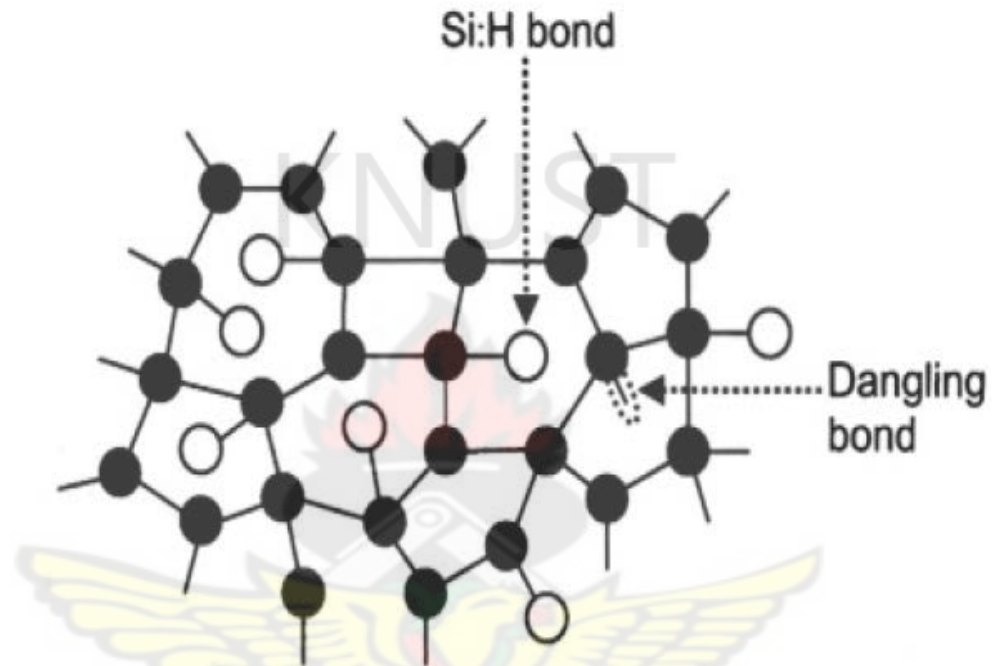


Figure 3.3. Schematic illustration of a two-dimensional continuous random network of atoms having various bonding coordination.

As mentioned above, in amorphous semiconductors, the allowed energy bands have band tails in the energy gap (Yacobi, B.G., 2004). Consider a degenerate direct band gap p-type semiconductor. One can excite electrons from states below the Fermi level, E_f , in the valence band where the band is nearly parabolic, to tail states below conduction band edge, E_c , where the density of states decreases exponentially with

energy into the band gap, away from E_c . Such excitations lead to absorption coefficient, α , depending exponentially on photon energy, $h\nu$, a dependence that is usually called the Urbach rule, given by

$$\alpha = \alpha_0 \exp [(h\nu - E_0)/\Delta E] \quad (3.0.1)$$

where α_0 and E_0 are material-dependent constants and ΔE , called the Urbach width, is also a material-dependent constant. The Urbach rule was originally reported for alkali halides. It has been observed for many ionic crystals, degenerately doped crystalline semiconductors and almost all amorphous semiconductors. While exponential band tailing can explain the observed Urbach tail of the absorption coefficient vs. photon energy, it is also possible to attribute the absorption tail behaviour to strong internal fields arising, for example, from ionized dopants or defects. Temperature-induced disorder in the crystal is yet another important mechanism that leads to an Urbach exponential absorption tail (Singh, J., 2006). The typically observed exponential energy dependence of the absorption edge or the Urbach edge provides an important parameter for characterizing the material's quality and it usually depends on the deposition method and deposition conditions. Thus as already noted above, in amorphous materials the exponential band tails are related to the structural disorder, i.e., bond length and bond angle deviations that broaden the distribution of electronic states; hence, the slope of the Urbach edge can be related to the material's quality (Street, 1991).

3.1. OPTICAL PROPERTIES OF FILM MATERIALS

Optical properties of semiconductors typically consist of their refractive index n and extinction coefficient k or absorption coefficient α (or equivalently the real and

imaginary parts of the relative permittivity) and their dispersion relations, that is their dependence on the wavelength, λ , of the electromagnetic radiation or photon energy $h\nu$, and the changes in the dispersion relations with temperature, pressure, alloying, impurities, etc. A typical relationship between the absorption coefficient and photon energy observed in a crystalline semiconductor is shown in figure 3.4, where various possible absorption processes are illustrated (Singh, J., 2006). The important features in the α vs. $h\nu$ behaviour as the photon energy increases can be classified in the following types of absorptions: (a) *Reststrahlen or lattice absorption* in which the radiation is absorbed by vibrations of the crystal ions, (b) *free-carrier absorption* due to the presence of free electrons and holes, an effect that decreases with increasing photon energy, (c) *an impurity absorption band* (usually narrow) due the various dopants, (d) *exciton absorption peaks* that are usually observed at low temperatures and are close to the fundamental absorption edge and (e) *band-to-band or fundamental absorption* of photons, which excites an electron from the valence to the conduction band (Singh, J., 2006).

The *fundamental absorption process*, probably the most important absorption effect, involves the absorption of photons, which have energies equal to or greater than the band gap energy. The fundamental absorption process is usually accompanied by an electronic transition across the forbidden gap and as a result, excess electron-hole pairs are generated in the semiconductor. The fundamental absorption manifests itself by a rapid rise in absorption and can be used to determine the band-gap energy of semiconductors and insulators.

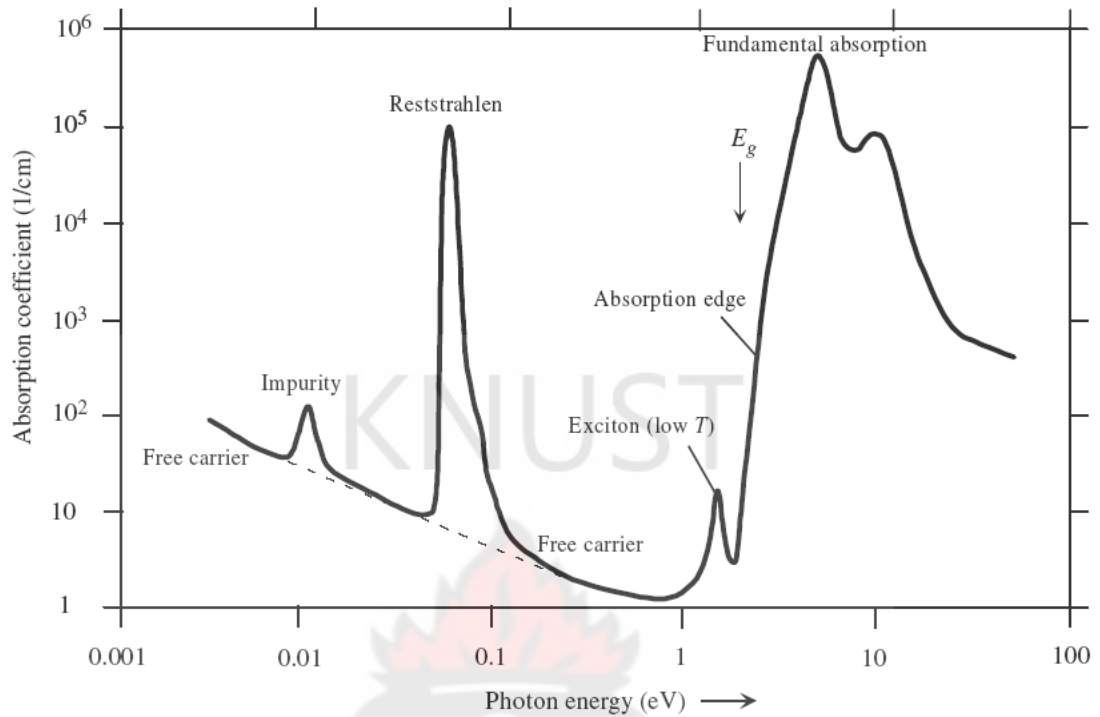


Figure 3.4 Absorption coefficient is plotted as a function of the photon energy in typical semiconductor to illustrate various possible absorption processes.

The absorption coefficient due to the interband transition is usually very large. However, the absorption coefficient becomes very small ($<1\text{cm}^{-1}$) when the photon energies fall below the band gap energy. In this case, another type of optical absorption process takes place which results in electronic transitions only within the allowed energy band and is called the *free-carrier absorption process*. This type of absorption result in the excitation of lattice phonons, accelerate free electrons in the conduction band or creation of an exciton (Li, S.S., 2006).

In order to understand the optical behaviour of films, one must become familiar with the optical constants of materials, their origins, magnitudes and how they depend on the way films are processed. The unifying concept that embraces all optical properties is the interaction of electromagnetic radiation with the electrons of the

material. On this basis, optical properties are interpretable from what we know of the electronic structure and how it is affected by atomic structure, bonding, impurities, and defects (Ohring, M., 1992).

3.1.1. OPTICAL MAGNITUDES AND THE DIELECTRIC CONSTANTS

Electromagnetic radiation propagates differently in materials than in free space because of the presence of charge. As a result, there is a change in the wave velocity and intensity of the radiation described by the complex index of refraction

$$N = n - ik \quad (3.1.1)$$

The quantity n is the real index of refraction and k is the index of absorption, which is also known as the extinction coefficient. These are the two material optical constants of concern here. The spatially dependent portion of the electric field of a wave propagating in the x direction is then expressed by.

$$E = E_0 \exp\left(-\frac{i2\pi Nx}{\lambda}\right) = E_0 \exp\left(-\frac{2\pi kx}{\lambda}\right) \exp\left(-\frac{i2\pi nx}{\lambda}\right) \quad (3.1.2)$$

Where E_0 is the field amplitude when $x = 0$ and λ is the wavelength. The real function $\exp\left(-\frac{2\pi kx}{\lambda}\right)$ represents an exponential damping or attenuation of the wave due to some absorption process within the material. On the other hand, the imaginary exponential portion of Eq. (3.1.2) contains n and reflects propagation without absorption. All materials exhibit varying proportion of these two linked attributes of N . In the highly absorbing metals, for example, n is usually small compared with k . On the other hand, the dielectric films used for optical purposes are highly nonabsorbing and k is vanishingly small compared with n . Multiplying E by its complex conjugate leads to the

well-known expression for the attenuation of the intensity, $I \propto EE^*$ or $I \propto E_0^2 \exp-4\pi kx/\lambda$. therefore (Ohring, M., 1992).,

$$I = I_0 \exp-\alpha x \quad (3.1.3)$$

where the absorption coefficient α is defined as $4\pi k/\lambda = 2\omega k/c$ and I_0 is the intensity of incident radiation, c is the speed of light.

Of the total radiation energy incident on an object, a fraction R is reflected from the top surface and a fraction T is transmitted through the bottom surface. The remaining fraction is lost through electronic absorption (A) processes and by scattering (S) at surface and volume imperfections. Surface roughness, internal boundaries and density fluctuations arising from porosity, pinholes, microcracks, particulate incorporation and impurities are sources of scattering. Adding the various contributions gives

$$R + T + A + S = 1 \quad (3.1.4)$$

For light passing through a medium of refractive index n_0 , impinging normally on a transparent film of index n_1 ,

$$R = \left(\frac{n_1 - n_0}{n_1 + n_0}\right)^2 \quad (3.1.5)$$

If, however, the film is absorbing with index of absorption k_1

$$R = \frac{(n_0 - n_1)^2 + k_1^2}{(n_0 + n_1)^2 + k_1^2} \quad (3.1.6)$$

The well known Maxwell's formula for the refractive index of a substance is $N = \sqrt{\epsilon \mu}$, where ϵ is the static dielectric constant or relative permittivity and μ the relative permeability. As $\mu = 1$ for nonmagnetic substances, one gets $N = \sqrt{\epsilon}$. As ϵ depends on the wavelength of light, the refractive index also depends on the wavelength

of light, and this dependence is called *dispersion*. The complex refractive index is related to the complex relative permittivity, $\varepsilon = \varepsilon_1 - i\varepsilon_2$, by:

$$N = n - ik = \sqrt{\varepsilon} = \sqrt{\varepsilon_1 - i\varepsilon_2} \quad (3.1.7)$$

where ε_1 and ε_2 are, respectively, the real and imaginary parts of ε . Eq. (2.4.7) gives:

$$n^2 - k^2 = \varepsilon_1 \text{ and } 2nk = \varepsilon_2 \quad (3.1.8)$$

In explicit terms, n and k can be obtained as (Singh, J., 2006):

$$n = \left[\frac{1}{2} \left((\varepsilon_1^2 + \varepsilon_2^2)^{1/2} + \varepsilon_1 \right) \right]^{1/2} \quad (3.1.9)$$

$$k = \left[\frac{1}{2} \left((\varepsilon_1^2 + \varepsilon_2^2)^{1/2} - \varepsilon_1 \right) \right]^{1/2} \quad (3.1.10)$$

3.1.2. ELECTRONIC TRANSITIONS IN SEMICONDUCTORS

There are two types of optical transition associated with the fundamental absorption process, namely, direct and indirect band-to-band transitions, as shown in Fig. 3.5.a and b. Since the photon momentum is small compared with the crystal momentum, the absorption process should essentially conserve the electron momentum, i.e., $\hbar k$. The direct (or vertical) transition shown in Fig. 3.5a is the dominant absorption process taking place in a direct band gap semiconductor like GaAs, where the conduction band minimum and the valence band maximum are located at the same k -value in the reciprocal space. For an indirect band gap semiconductor (e.g., Si, Ge), the conduction band minimum and the valence band maximum are not located at the same k -value in the reciprocal space as shown in Fig. 3.5b. Therefore, the indirect optical transition induced by photon absorption is usually accompanied by the simultaneous absorption or emission of a phonon to conserve momentum; the probability of such a

process is substantially lower compared with direct transitions (Li, S.S., 2006). Therefore, in general, fundamental absorption in indirect gap semiconductors is relatively weaker as compared with the direct gap materials.

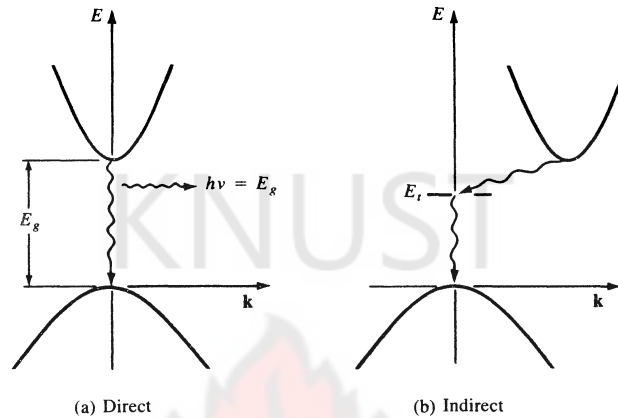


Figure 3.5. Direct and indirect electron transitions in semiconductors (a) Direct transition with accompanying photon emission; (b) indirect transition via a defect level.

3.1.3. IMPURITY ABSORPTION

Impurity absorption can be registered as the peaks of absorption coefficient lying below the fundamental (band-to-band) and excitonic absorption. Mostly they can be related to the presence of ionized impurities or, simply, ions. The origin of these peaks lies in the electronic transitions either between electronic states of an ion and conduction/valence band or intra-ionic transitions (e.g., within d or f shells, or between s and d shells, etc.). In the first case the appearing features are intense and broad lines while in the latter case their appearance strongly depends on whether these transitions are allowed or not by the parity selection rules. For allowed transitions the appearing absorption peaks are quite intense and broad while the forbidden transitions produce weak and narrow peaks. (Singh, J., 2006)

3.1.4. OPTICAL ABSORPTION AND BAND GAP

The optical absorption is described by an absorption coefficient α , which can be derived from transmission or absorption measurements. If I_0 is an incident light intensity, I is the transmitted light intensity and R is the reflectivity, then the transmission, $T = I/I_0$ can be written as (neglecting interference)

$$T = \frac{(1-R)^2 \exp(-\alpha t)}{1-R^2 \exp(-2\alpha t)} \quad (3.1.11)$$

where t is the thickness of the material. For large αt , this expression can be reduced to

$$T = (1-R)^2 \exp(-\alpha t) \quad (3.1.12)$$

and, in the absence of reflection, it can be further reduced to

$$I = I_0 \exp(-\alpha t) \quad (3.1.13)$$

In terms of absorbance A ,

$$\alpha = \frac{1}{t} (2.303 * A) \quad (3.1.14)$$

The relation between the absorption coefficient and the incident photon energy in a direct transition is given by

$$\alpha h\nu = A(h\nu - E_g)^n \quad (3.1.15)$$

where A is a constant, E_g is the optical energy gap. The value of n is $1/2, 3/2$ for direct allowed and direct forbidden transitions respectively. Thus, a plot of $(\alpha h\nu)^2$ versus $h\nu$ allows one to determine the energy gap (Tauc, J., 1974; Yacobi, B.G., 2004).

The optical absorption coefficient due to the indirect transitions with phonon

absorption is

$$\alpha_a = \frac{A(h\nu - E_g + E_p)^2}{(\exp(E_p / k_B T) - 1)} \quad (3.1.16)$$

E_p is the phonon energy. Similarly, for transitions involving phonon emission is

$$\alpha_e = \frac{A(h\nu - E_g + E_p)^2}{(1 - \exp(-E_p / k_B T))} \quad (3.1.17)$$

Meaning the optical absorption coefficient for the indirect allowed transitions varies with the square of the photon energy. A plot of $\alpha^{1/2}$ versus $h\nu$ at different at different temperatures should yield a straight line, and its intercept with the horizontal axis allows one to determine the phonon and the energy band gap of a semiconductor.

3.2. THE PHOTOCONDUCTIVITY EFFECT

Photoconductivity processes involve the absorption of energy from light or from particles, the excitation of charge carriers from a nonconducting ground state to a higher energy state where they are free to contribute to the electric conductivity and the return of charge carriers from the conducting state to ground state (Bube, R. H., 1960).

In the absence of illumination, the dark conductivity of a semiconductor is given by

$$\sigma_0 = q(n_0\mu_n + p_0\mu_p) \quad (3.2.1)$$

where q is the electronic charge, n_0 and p_0 denotes the densities of electrons and holes in thermal equilibrium, while μ_n and μ_p are the electron and hole mobilities, respectively.

When photons with energies equal to or greater than the band gap energy are absorbed in a semiconductor, intrinsic photoconductivity results. The absorbed photons create excess electron-hole pairs and as a result the densities of electrons and holes increase above the equilibrium values of n_0 and p_0 (i.e., $n = n_0 + \Delta n$, $p = p_0 + \Delta p$). Photoconductivity is defined as the net change in electrical conductivity under illumination and can be expressed by

$$\Delta\sigma = \sigma - \sigma_0 = q(\Delta n\mu_n + \Delta p\mu_p) \quad (3.2.2)$$

where Δn and Δp are the excess electron and hole densities, respectively. In a degenerate semiconductor, Δn and Δp are generally much smaller than n_0 and p_0 , and the effect of incident photons can be considered as a small perturbation. However, in an insulator or a nondegenerate semiconductor, values of Δn and Δp can become comparable or larger than their equilibrium carrier densities. If the effect of electron or hole trapping by the defect levels is negligible and the semiconductor remains neutral under illumination, then $\Delta n = \Delta p$ holds throughout the specimen (Li, S.S., 2006).

The other type of photoconduction process is known as extrinsic photoconductivity, in which electrons (or holes) are excited from the localised donor (or acceptor) states into the conduction (valence) band states by the absorption of photons with energy equal or greater than the activation energy of the donor (or acceptor) levels, but is less than the band gap energy of the semiconductor.

In intrinsic photoconduction, both the photogenerated electrons and holes participate in the photoconduction process and the photoconductivity is described by (3.2.2). However, in extrinsic photoconductors usually operated at cryogenic temperatures, the photoconduction process usually involves only one type of charge carrier and the expressions for the extrinsic photoconductivity are given by

$$\Delta\sigma_n = qn_D \mu_n \quad \text{for n-type} \quad (3.2.3a)$$

$$\Delta\sigma_p = qp_A \mu_p \quad \text{for p-type} \quad (3.2.3b)$$

where n_D and p_A are the photogenerated excess electron and hole densities from the donor and acceptor centers respectively.

The rate of generation of electron-hole pairs per unit volume per unit time can be written as

$$g_E = \alpha\Phi_0(1 - R) \quad \text{for } \alpha t \ll 1 \quad (3.2.4)$$

$$g_E = \alpha\Phi_0(1 - R)^{\alpha y} \quad \text{for } \alpha t \ll 1 \quad (3.2.5)$$

where R is the reflection coefficient of the semiconductor defined by (3.1.6), α is the absorption coefficient, Φ_0 is the photon flux density (i.e., $\Phi_0 = I_0 / hv$) and I_0 is the incident light intensity per unit area (W/cm^2).

For a very thin photoconductor in which photons are uniformly absorbed throughout the sample Eq. (3.2.4) is valid, while Eq. (3.2.5) is applicable for a thick specimen in which the photogeneration rate decays exponentially with penetration distance (Li, S.S., 2006).

In the former case of a thin specimen with $\alpha t \ll 1$. Here, the excess electron and hole densities are related to the generation rate g_E by

$$\Delta n = g_E \tau_n \quad (3.2.6)$$

$$\Delta p = g_E \tau_p \quad (3.2.7)$$

where τ_n and τ_p denote the electron and hole lifetimes respectively.

As shown in Figure 3.6, the change of electrical conductance as a result of the incident photons can be expressed by

$$\begin{aligned} \Delta G &= \Delta \sigma \left(\frac{A}{l} \right) = q(\Delta n \mu_n + \Delta p \mu_p) \left(\frac{Wt}{l} \right) \\ &= q g_E (\tau_n \mu_n + \tau_p \mu_p) \left(\frac{Wt}{l} \right) \end{aligned} \quad (3.2.8)$$

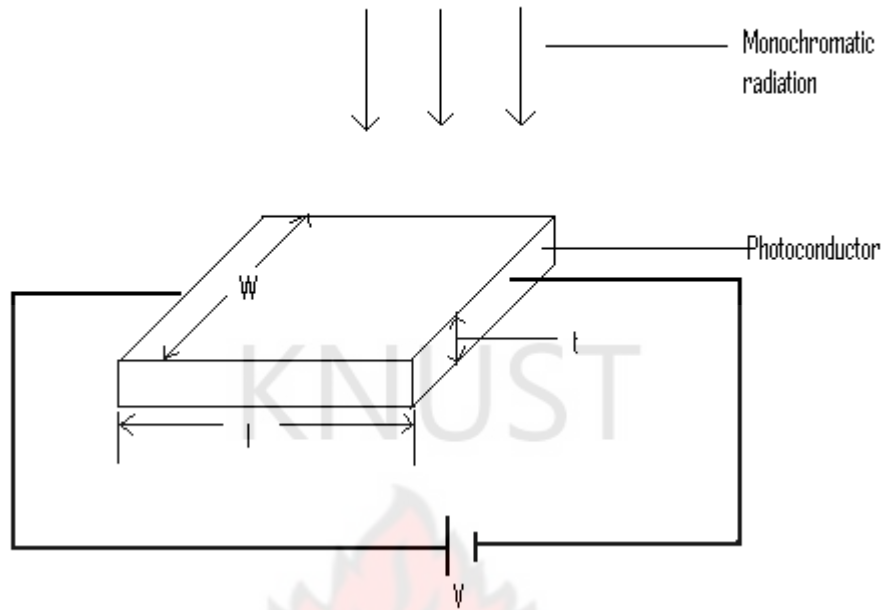


Figure 3.6. Photoconductivity process in a semiconductor specimen.

and

$$\Delta G = qG_E \frac{(\tau_n \mu_n + \tau_p \mu_p)}{l^2} \quad (3.2.9)$$

where $G_E = g_E(Wtl) = g_E V_0$ is the total volume generation rate (i.e., total number of carriers generated per second) and $A = Wt$ is the cross-sectional area. If V is the applied voltage, the photocurrent I_{ph} can be expressed as

$$I_{ph} = V\Delta G = qVG_E \frac{(\tau_n \mu_n + \tau_p \mu_p)}{l^2} = qVG_E S \quad (3.2.10)$$

where

$$S = \frac{(\tau_n \mu_n + \tau_p \mu_p)}{l^2} = \frac{\mu\tau}{l^2} \quad (3.2.11)$$

is the photosensitivity factor. It is seen that the value S is directly proportional to the product of $\mu\tau$. This means that in order to obtain a high photosensitivity factor, the lifetimes and mobilities of the excess carriers must be as large as possible and the sample length l between two electrodes should be as small as possible (Li, S.S., 2006).

KNUST



CHAPTER FOUR

4. EXPERIMENTAL DETAILS

4.0. REAGENTS

The starting chemicals in the preparation of the films consisted of aqueous solutions of concentrated hydrochloric acid, concentrated nitric acid, for degreasing the glass slides to be used as substrate. Zinc nitrate $Zn(NO_3)_2 \cdot 6H_2O$, cadmium nitrate $Cd(NO_3)_2 \cdot 4H_2O$ and thiourea, $(NH_2)_2CS$ in methanol were used for the films formation. The chemicals were obtained from BDH chemicals Poole, England.

4.0.1. 0.25M ZINC NITRATE SOLUTION ($Zn(NO_3)_2$)

Zinc nitrate (3.7185 g) was measured into a into a 50ml volumetric flask and diluted to the mark with methanol. The resulting solution had a concentration of 0.25M.

4.0.2. 1.0 M CADMIUM NITRATE SOLUTION ($Cd(NO_3)_2$)

Cadmium nitrate (15.425 g) was measured into a into a 50ml volumetric flask and diluted to the mark with methanol. The resulting solution had a concentration of 1.0 M.

4.0.3. 0.375 M CADMIUM NITRATE SOLUTION ($Cd(NO_3)_2$)

18.75ml of 1.0M cadmium nitrate solution was measured into 50ml volumetric flask and diluted to the mark with methanol. The resulting solution had a concentration of 0.375M.

4.0.4. 0.1667 M CADMIUM NITRATE SOLUTION (Cd(NO₃)₂)

8.33ml of 1.0M cadmium nitrate solution was measured into 50ml volumetric flask and diluted to the mark with methanol. The resulting solution had a concentration of 0.1667M.

4.0.5. 0.0625 M CADMIUM NITRATE SOLUTION (Cd(NO₃)₂)

3.125ml of 1.0M cadmium nitrate solution was measured into 50ml volumetric flask and diluted to the mark with methanol. The resulting solution had a concentration of 0.0625M.

4.0.6. 0.5M THIOUREA SOLUTION ((NH₂)₂CS)

Thiourea ((NH₂)₂CS), (1.903 g) was measured into a 50ml volumetric flask and diluted to the mark with methanol. The resulting solution had a concentration of 0.5M.

4.1. SURFACE PREPARATION OF SUBSTRATES

A clean surface is one that contains no significant amount of undesirable material (Mattox, D. M., 1978). Cleaning is defined as the removal, by physical and or chemical means, of soil that could interfere with the preparation of the desired material. Soil is matter on the surface whose chemical characteristics are different from those being formed. The types of soils most commonly encountered are fingerprint oils, metal oxides, dirt, etc. (Beal, S. E., 1978). The nature and surface finish of the substrates are extremely important because they greatly influence the properties of films deposited on them (Chopra, K. L., 1969). It is therefore important that prior to the deposition of the semiconducting thin film the substrate, in this case, microscope glass slide is cleaned thoroughly to remove any undesirable substance from it. The glass slides were left in a

solution of Aqua Regia (3 parts HCl: 1 part HNO₃), for about 24 hours to remove any grease. They were then cleaned with detergent and rinsed with distilled water before use.

4.2. SAMPLE PREPARATION

The Cadmium Nitrate was the source of cation (Cd²⁺), Zinc Nitrate was the source of another cation (Zn²⁺), and thiourea was the source of anion S²⁻. By varying the relative ratio of Cd and Zn ions using Eq. (4.2.1), Cd_{1-x}Zn_xS thin films with solution composition parameter x= 0.2, 0.4, 0.6, 0.8 were deposited on the glass substrates. From Song, *et al.*, 2005

$$x \text{ is defined as } = \frac{[\text{Zn}(\text{NO}_3)_2]}{[\text{Zn}(\text{NO}_3)_2] + [\text{Cd}(\text{NO}_3)_2]} \quad (4.2.1)$$

Table1.1. Combination of the various ion concentrations employed in the preparation of the samples.

Composition parameter, x.	Concentration Cd(NO ₃) ₂ .4H ₂ O / M	Concentration Zn(NO ₃) ₂ .6H ₂ O / M	Concentration (NH ₂) ₂ CS / M
0.2	1.0000	0.2500	0.5
0.4	0.3750	0.2500	0.5
0.6	0.1667	0.2500	0.5
0.8	0.0625	0.2500	0.5

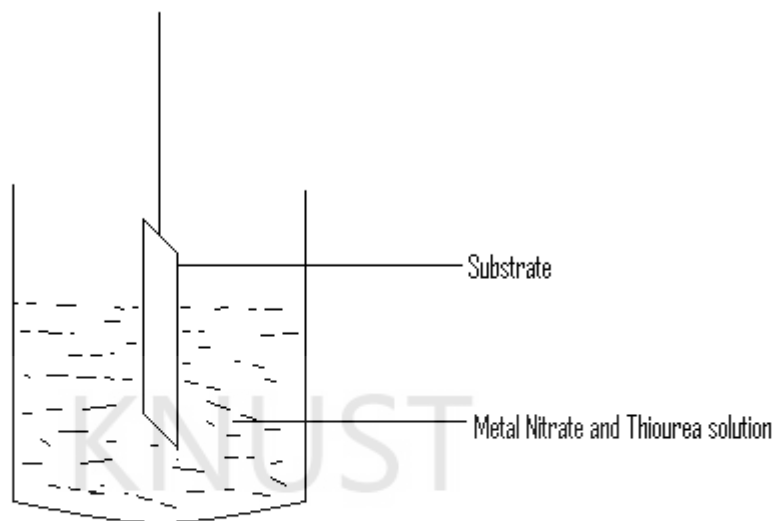


Figure 4.1. Experimental Set-up for thin film deposition by the dip technique

The experimental arrangement was as shown in figure 4.1. The substrate was withdrawn vertically from a methanol solution of cadmium nitrate, zinc nitrate and thiourea at a controlled speed. The substrate was then transferred into an oven at a temperature of about 85°C and baked for about five minutes. The reactions taking place are typically



where the compounds CdS and ZnS conflate in the ratio (1-x) : x to form the alloy

$\text{Cd}_{1-x}\text{Zn}_x\text{S}$. The subscript x is the composition parameter defined by Eq. (3.1)

The thickness of the deposited films was measured by weight difference method using a sensitive electronic balance.

An initial attempt to deposit the films using smaller concentrations than in the table 1.1 above resulted only in ultra thin films whose thickness the gravimetric method could not determine, after several dipping and baking, only the sample with high cadmium concentration could form some appreciable film. This necessitated the preparation of higher concentrations that is shown in the table 1.1 above.

In the end, films varying from yellow ($x = 0.2$) to almost white ($x = 0.8$) in colour were obtained.

4.3. THE MEASUREMENT OF ABSORPTION SPECTRA

Absorption spectra are usually registered by instruments known as spectrophotometers. Figure 4.2 shows a schematic diagram with the main elements of the simplest spectrophotometer. Basically, it consists of the following components: (i) a light source (usually a deuterium lamp for the UV spectral range and a tungsten lamp for the VIS and IR spectral ranges) that is focused on the entrance to (ii) a monochromator, which is used to select a single wavelength (frequency) from all of those provided by the lamp source and to scan over a desired frequency range. (iii) a sample holder, followed by (iv) a light detector, to measure the intensity of each monochromatic beam after traversing the sample and finally (v) a computer, to display and record the absorption spectrum (Sole, J. G., *et al.*, 2005).

The LKB ultrospecII 4050 UV/Visible spectrophotometer used in this work had all the elements but the computer unit. A glass slide that had been treated the same way as the slides with films but with no film on it was used as the reference slide. The wavelength was varied in units of 10 from 300nm to 900nm and the corresponding absorbance reading recorded.

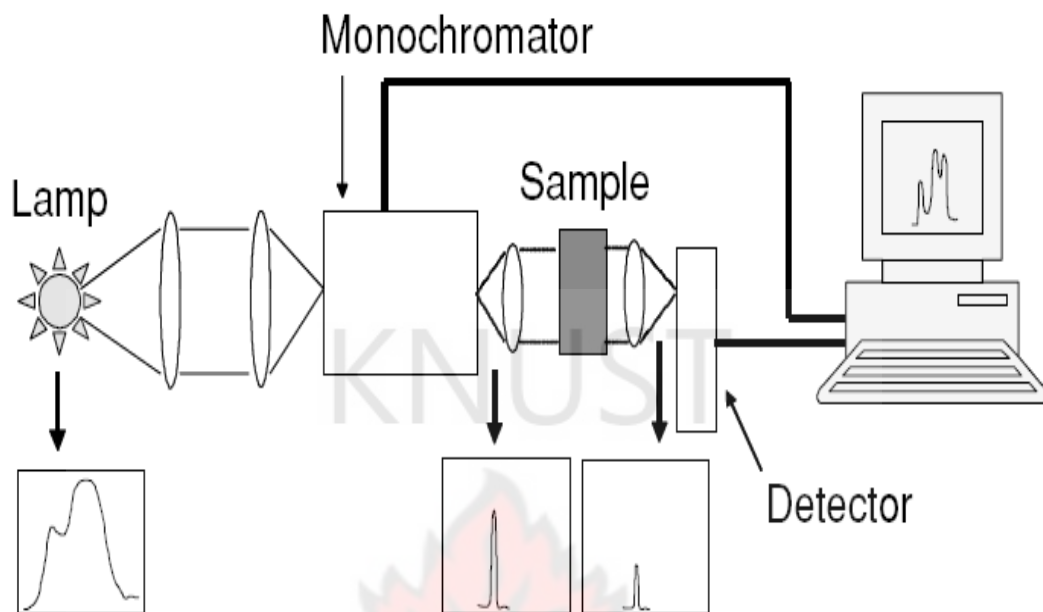


Figure 4.2 Schematic diagram of a single-beam spectrophotometer.

Aside the absorbance of the as deposited films, the samples were thermally annealed for one hour at temperatures of about 100°C, 200°C, 300°C and the absorbance again recorded.

4.4. THE MEASUREMENT OF FILM THICKNESS

The thickness of a film is among the first quoted attributes of its nature. The reason is that thin film properties and behaviour depend on thickness. Decorative, metallurgical, protective films and coatings are some applications where film thickness is not particularly crucial to function. On the other hand, microelectronic applications generally require the maintenance of precise and reproducible film thicknesses as well as

lateral dimensions. Even more stringent thickness requirements must be adhered to in optical applications, particularly in multilayer coatings (Ohring, M., 1992).

The varied types of films and their uses have generated a multitude of ways (optical and mechanical) to measure film thickness. A list of some methods is given in table 1.2 with typical measurement ranges and accuracies. Included are destructive and nondestructive methods. The overwhelming majority are applicable to films that have been prepared and removed from the deposition chamber. Only a few are suitable for real-time monitoring of film thickness during growth (Ohring, M., 1992).

Table 1.2. A Summary of Selected Film Thickness Measurement Techniques

Method	Range	Accuracy or Precision	Comments
Multiple-beam FET	30–20,000 Å	10–30 Å	A step and reflective coating required
Multiple-Beam FECO	10–20,000 Å	2 Å	A step, reflective coating, and spectrometer required; accurate but time-consuming
VAMFO	800 Å–10 μm	0.02–0.05 %	For transparent films on reflective substrates; Nondestructive
CARIS	400 Å–20 μm	10 Å–0.1%	For transparent films; Nondestructive
Step gauge	500–15,000 Å	~ 200 Å	Values for SiO ₂ on Si
Ellipsometry	A few Å to a few μm	1 Å	Transparent films; complicated mathematical analysis
Stylus	20 Å to no limit	A few Å to < 3%	Step required; simple and rapid
Weight measurement	< 1 Å to no limit		Accuracy depends on knowledge of film density
Crystal oscillator	< 1 Å to a few μm	< 1 Å to a few %	Nonlinear behavior at larger film thicknesses

In this work the weight measurement method also called gravimetric technique was employed because of the lack of film thickness measuring equipment such as interferometers or stylus instruments. Knowing the film mass m , the deposit area A , and the film density ρ , the thickness t , is given as

$$t = \frac{m}{\rho * A} \quad (4.4.1)$$

To know the film mass means weighing the substrate before and after deposition and subtracting the mass before deposition from the mass after deposition with a precision mass balance. This method has a number of challenges in measuring film thickness because film density is not known with certainty. The reason is that the film packing factor P , a measure of the void content, can be quite low for porous deposits. Furthermore, the effective deposit area will be larger than the assumed in case the substrate contains a great deal of relief in the form of roughness, cleavage steps etc.

4.5. PHOTOCONDUCTIVITY TEST

The experimental set-up for the photoconductivity test is as shown in figure 4.3, comprising of a constant current source, load resistor R_1 of known resistance, and the sample in series, a light source, focusing lens and a voltmeter to measure voltage across the load resistor. The electrodes to the samples were joined with the help of silver paste to enhance ohmic contact formation.

The voltage across the load resistor was measured without and with illumination. Afterwards, the sample was irradiated with light of a particular wavelength with the aid of colour filters (Red, Orange, Yellow, Green, Blue, and Violet).

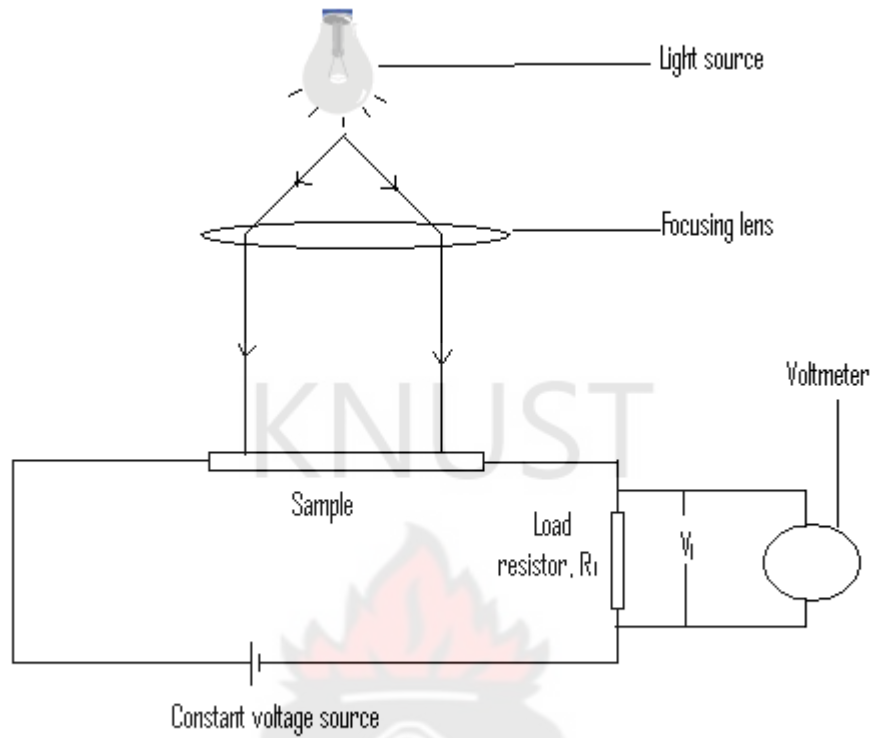


Figure 4.3. Schematic diagram of photoconductivity set-up

For each wavelength, the change in voltage across the resistor, i.e. voltage in the dark and voltage under illumination were measured. From Ohm's law the current through the circuit was deduced and the change in current with and without illumination gives the photocurrent.

CHAPTER FIVE

5. RESULTS AND DISCUSSION

The film adherence was good except the one with $x = 0.2$, i.e. the one with high cadmium content and the colours varied from yellow to white- yellowish, as the Zn- content increased in the sample. The calculated film thickness using the gravimetric method indicates that, generally, thicker films were formed with increasing Cd for the same number of dipping. The thickness of the films were $18.85\mu\text{m}$, $8.61\mu\text{m}$, $5.06\mu\text{m}$, $6.23\mu\text{m}$ for $x= 0.2, 0.4, 0.6, 0.8$ respectively. Tables (5.1-5.4) in appendix A show the absorbance reading of the as deposited as well as annealed samples. Using Eq. (3.1.14) the absorption coefficient, α , of the films were evaluated as a function of photon energy.

5.0. VARIATION OF ABSORPTION COEFFICIENT VERSUS ENERGY AT DIFFERENT ANNEALING TEMPERATURES

A plot of α against photon energy, $h\nu$, for samples with composition $x = 0.2, 0.4$ are displayed in figures 5.1 and 5.2 respectively. It can be seen from both figure 5.1 and 5.2 that there is a shift of the fundamental absorption edge towards long wavelengths, from blue to green of the optical spectrum as annealing temperature increase and also, raising the fundamental edge, leading to a high absorption coefficient. However, the shift is very small from $200\text{ }^{\circ}\text{C}$ to $300\text{ }^{\circ}\text{C}$ annealing temperatures in both films. Shifting of the absorption edge which lead to high absorption coefficient may be attributed to phase transformation (say from the cubic structure to hexagonal structure) or alternatively rearrangement of defect states as the heat treatment activates processes such as solid state diffusion in the film.

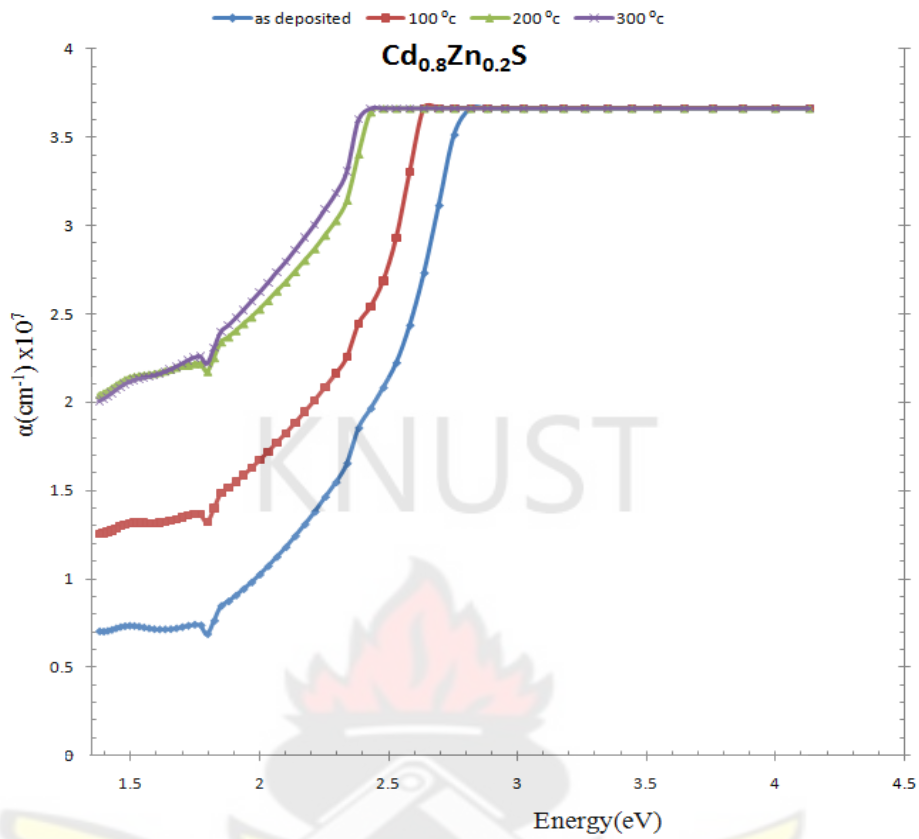


Figure 5.1 Absorption coefficient, α , versus photon energy, $h\nu$, for $\text{Cd}_{0.8}\text{Zn}_{0.2}\text{S}$ sample.

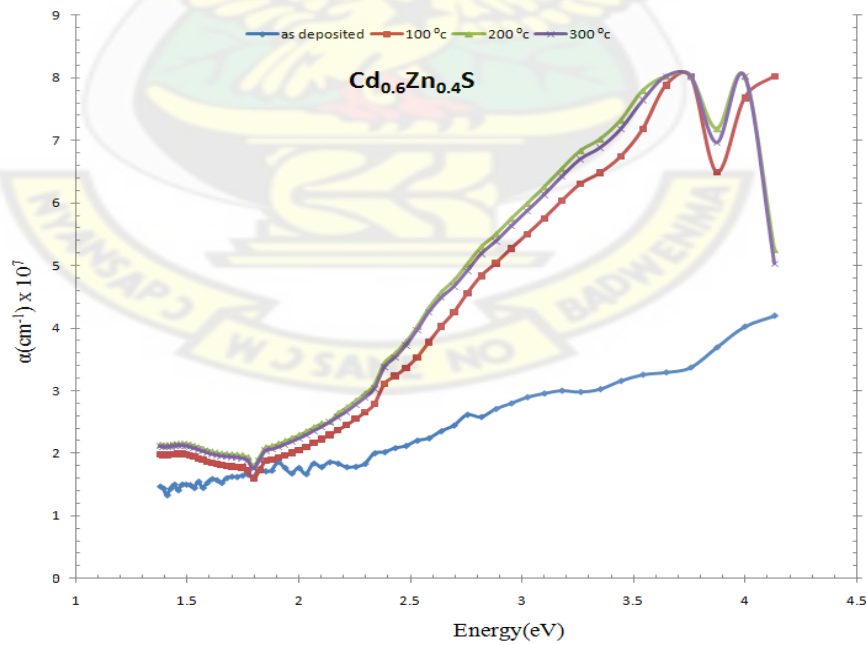


Figure 5.2 Absorption coefficient, α , versus photon energy, $h\nu$, for $\text{Cd}_{0.6}\text{Zn}_{0.4}\text{S}$ sample.

Again, surface oxides; which may have been formed during the annealing process could have also contributed to the increased absorption of the samples.

Annealing temperature did not exceed 300 °C because at 400 °C the samples became dark, possibly due to the organic solvent methanol that was used in their preparation and the relatively long annealing time.

The absorption of photon energy less than the band gap energy involves localised tail states and hence does not obey Eq. (3.1.15). Instead there was exponential dependence of absorption coefficient on photon energy giving rise to Urbach's tail. The Urbach's tail has been used to describe the extent of structural disorder in the sample, but the current understanding is that in amorphous solids it occurs due to both structural and thermal disorder (Cody, 1984).

5.1. OPTICAL BAND GAP

The electronic energy band parameters of semiconductor alloys and their dependence on alloy composition are very important. The energy band gap of a ternary alloy is dependent on the relative concentration of the constituent elements.

From the absorption spectra, the optical band gaps of the films were evaluated. The band gap (E_g) for allowed direct transition were evaluated by extrapolating the straight line portion of the $(ah\nu)^2$ vs $h\nu$ plot to $\alpha = 0$ and is shown in figure 5.3 for sample $Cd_{0.8}Zn_{0.2}S$ at three different annealing temperatures. Figure 5.4 and 5.5 show a similar plot for sample $Cd_{0.6}Zn_{0.4}S$ and $Cd_{0.4}Zn_{0.6}S$ respectively. Thermal annealing is found to decrease the optical band gap band gap of the films, for instance, band gap of

the sample $\text{Cd}_{0.8}\text{Zn}_{0.2}\text{S}$ varied from 2.42eV as-deposited to 2.12eV after annealing to 300 °C for one hour.

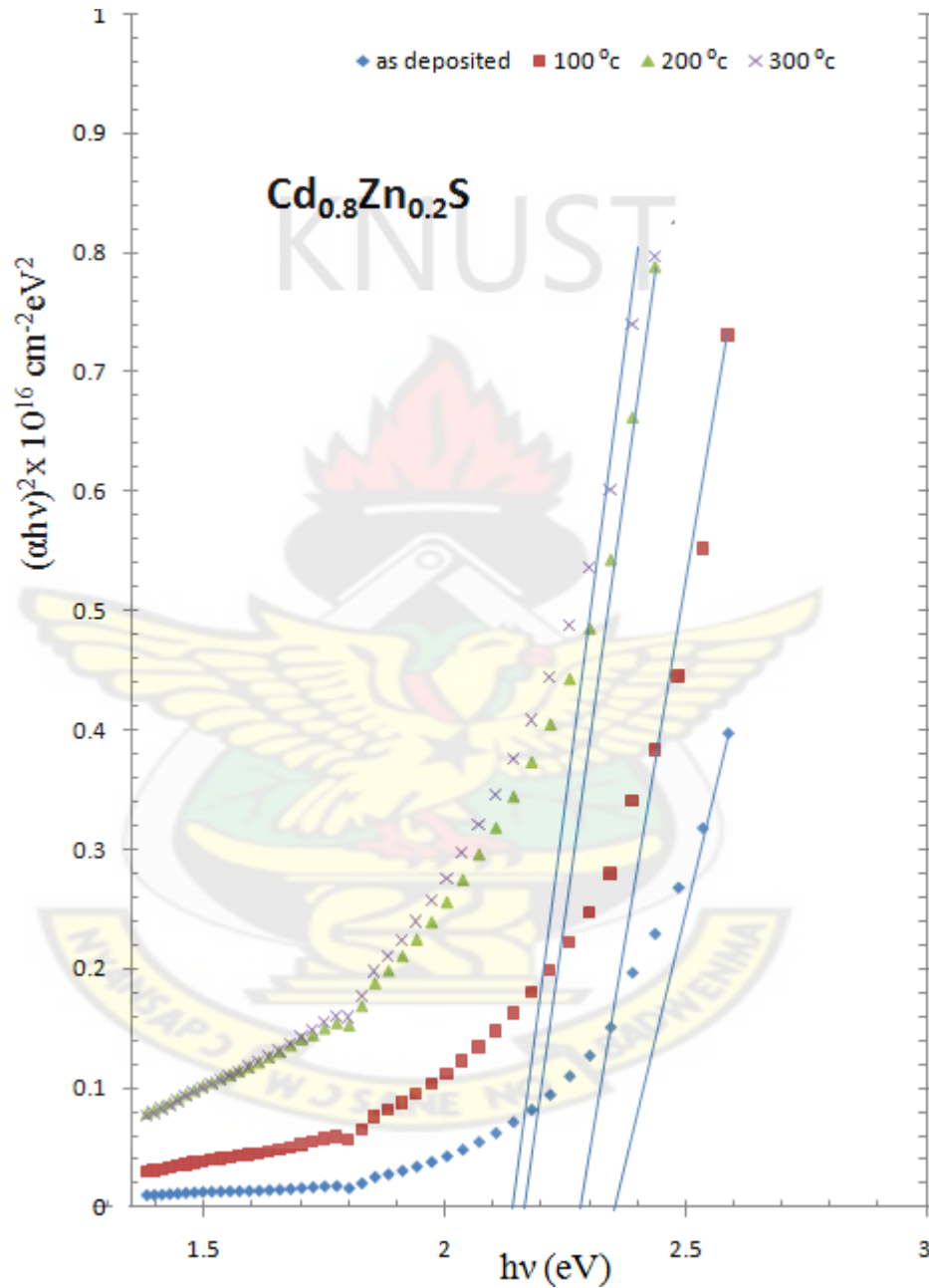


Figure 5.3 Square of absorption coefficient, α^2 , multiplied by square of photon energy, $(h\nu)^2$, plotted as a function of the photon energy, $h\nu$, for $\text{Cd}_{0.8}\text{Zn}_{0.2}\text{S}$ film annealed at different temperatures. Extrapolation of the straight region of the plot to $(\alpha h\nu)^2 = 0$ gives the optical band gap.

Also, the band gap of the sample $\text{Cd}_{0.6}\text{Zn}_{0.4}\text{S}$ varied from 3.36eV as-deposited to 2.60eV at 300 °C. The decreased band gap of the films after annealing may be due to improvement in the structure, i.e., improving crystallinity or alternatively, a phase transformation taking place in the samples as a result of the heat treatment. A similar effect of decreased band gap as a result of heat treatment of $\text{Cd}_{1-x}\text{Zn}_x\text{S}$ thin films for photovoltaic applications has been reported by (Chavhan, S.D., *et al.*, 2008). Again, an increase in grain size after annealing could also cause a decrease in the band gap of the sample.

Increasing Zn content in the sample increased the optical band gap from 2.42 (x = 0.2) to 3.61 (x = 0.8), just as it has been elaborated on in the literature review. A summary of the optical band gap values with the sample constituent and at the various annealing temperatures is shown in table 5.5 (appendix B).

A plot of the optical band gap, E_g , against Zn composition, x, when the samples had been annealed to 200 °C is shown in figure 5.6, the somewhat linear variation of E_g with sample composition is a sign of solid solution formation. That is, as Zn content increases in the sample the energy gap of the ternary $\text{Cd}_{1-x}\text{Zn}_x\text{S}$ approaches that of the binary ZnS which is quoted to be about 3.70eV. The band gap increase with Zn concentration makes $\text{Cd}_{1-x}\text{Zn}_x\text{S}$ suitable material for application as a buffer layer in Copper-Indium-Gallium-Selenide (CIGS) based solar cells than CdS, since the higher band gap (> 2.40 eV) for CdS will allow more short-wavelength photons to reach the absorber layer and generate photocurrent.

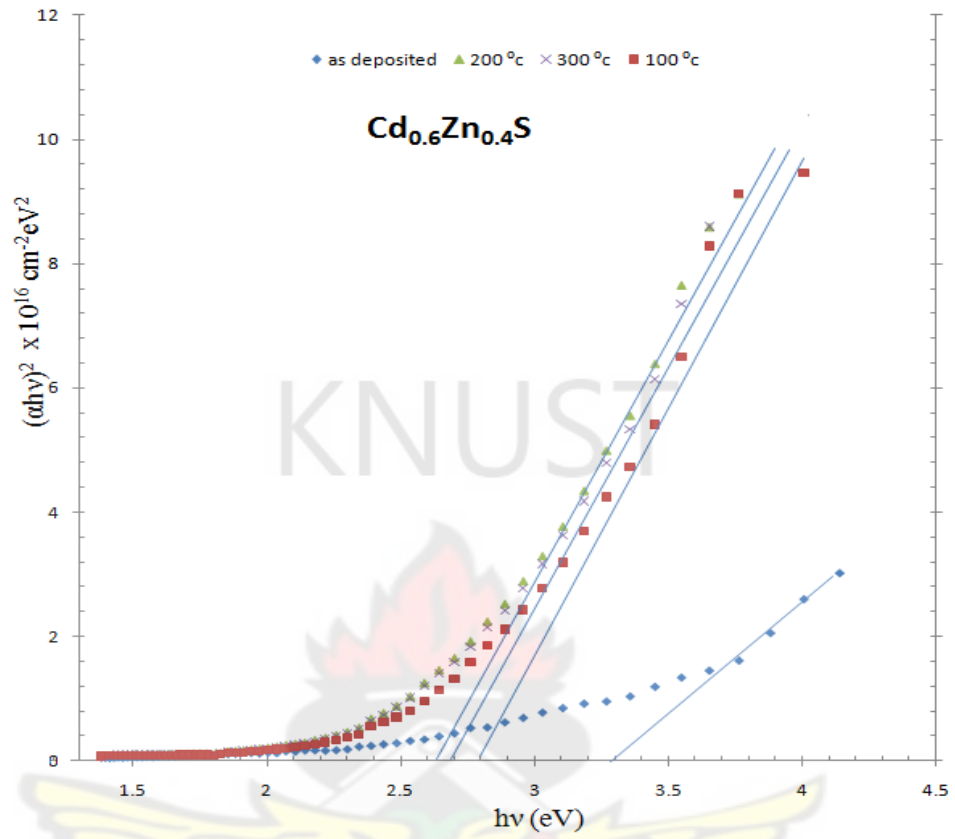


Figure 5.4 Square of absorption coefficient, α^2 , multiplied by square of photon energy, $(hv)^2$, plotted as a function of the photon energy, hv , for $Cd_{0.6}Zn_{0.4}S$ film annealed at different temperatures. Extrapolation of the straight region of the plot to $(\alpha hv)^2 = 0$ gives the optical band gap.

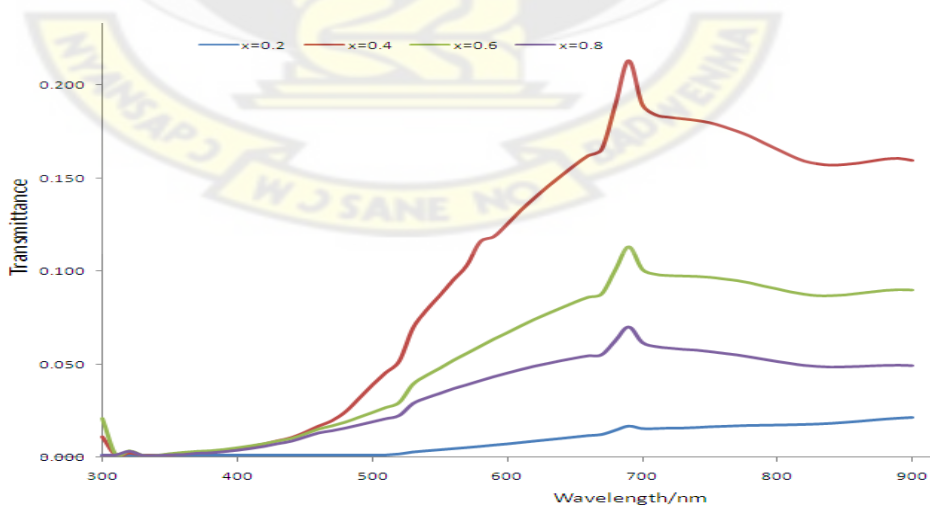


Figure 5.5 A plot of transmittance versus wavelength.

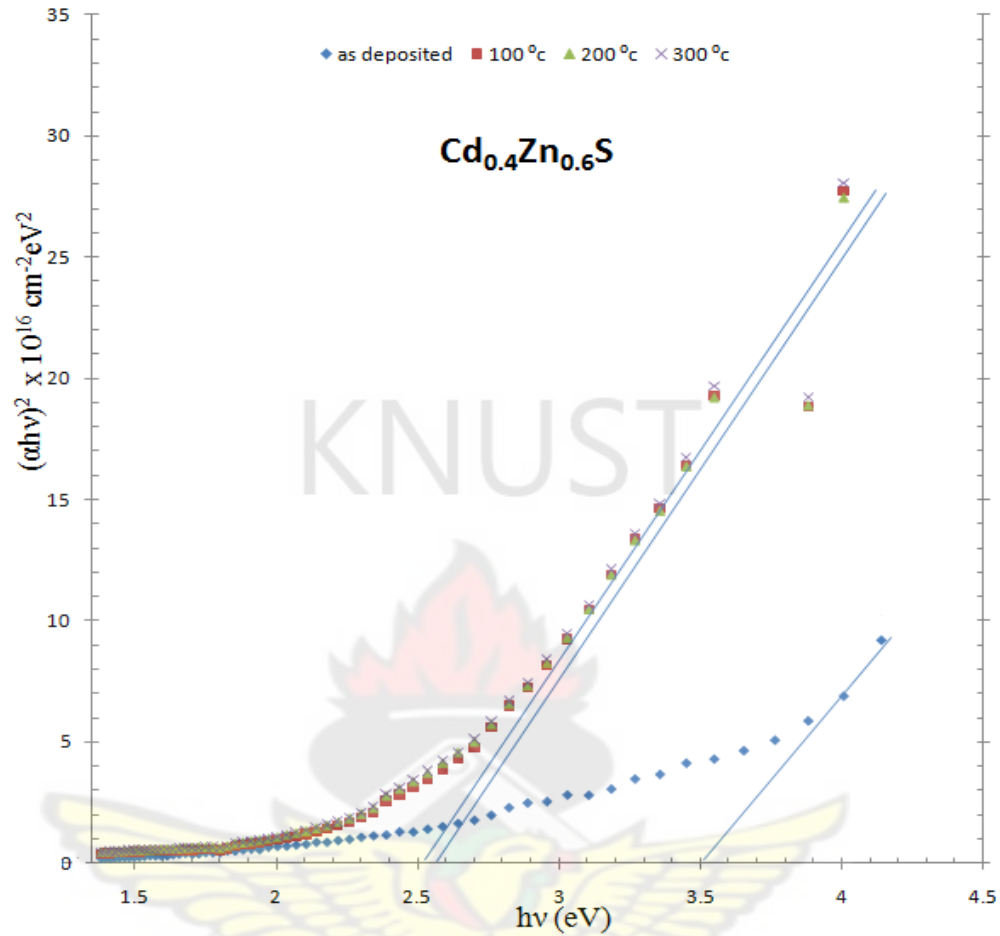


Figure 5.6 Square of absorption coefficient, α^2 , multiplied by square of photon energy, $(hv)^2$, plotted as a function of the photon energy, hv , for $Cd_{0.4}Zn_{0.6}S$ film annealed at different temperatures. Extrapolation of the straight region of the plot to $(\alpha hv)^2 = 0$ gives the optical band gap.

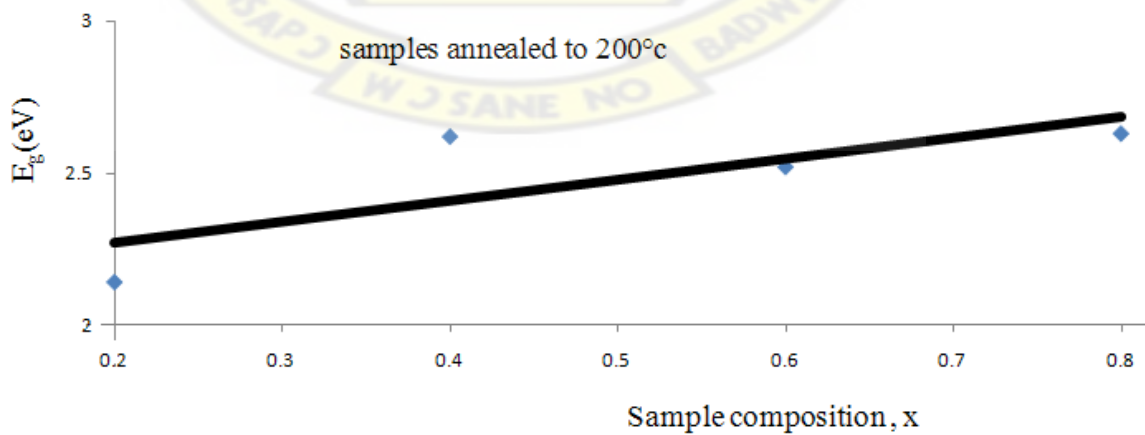


Figure 5.7 Optical band gap variation with zinc concentration in the samples

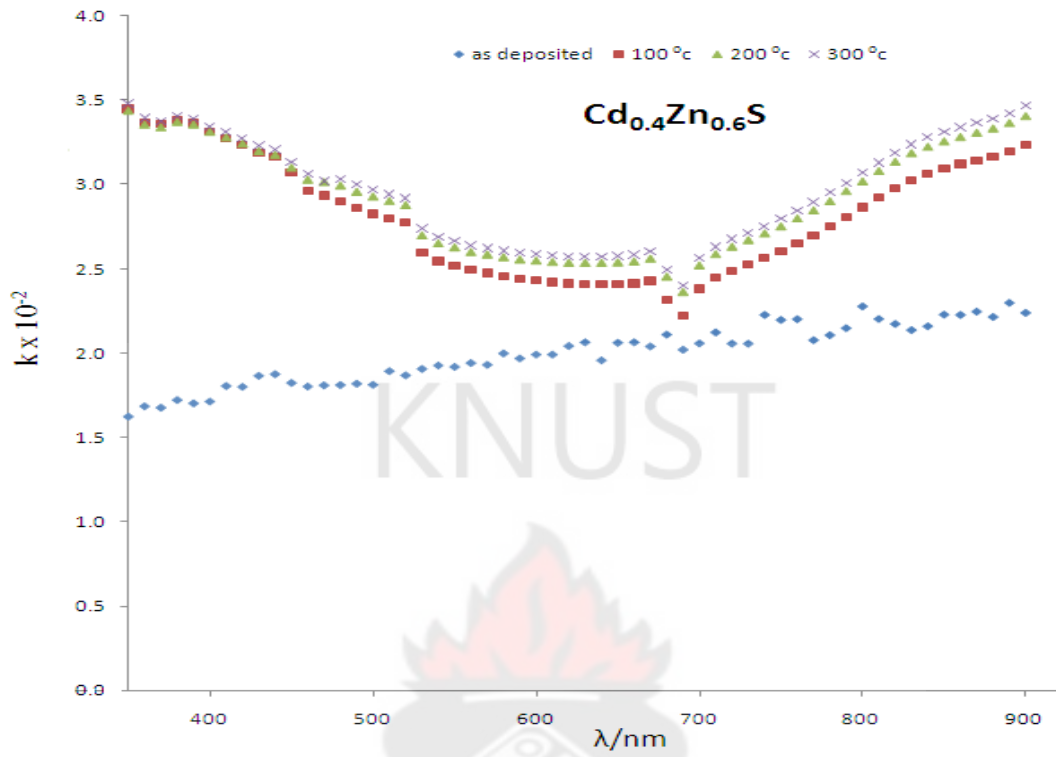


Figure 5.8 A plot of extinction coefficient versus wavelength for Cd_{0.4}Zn_{0.6}S sample.

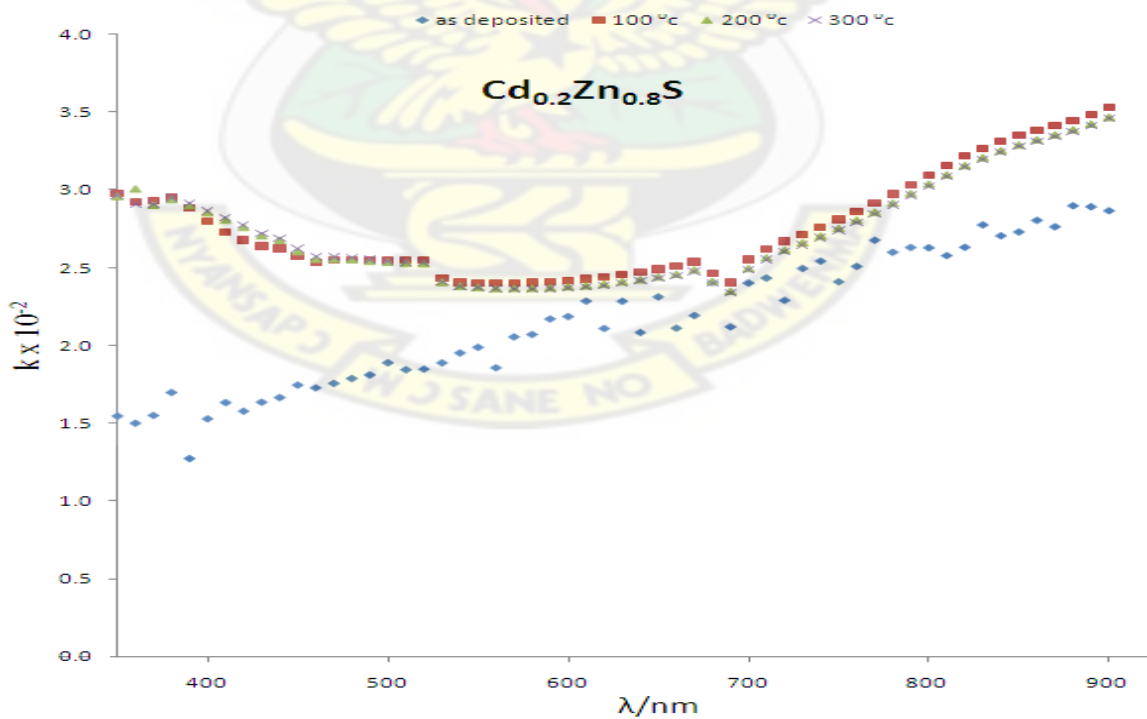


Figure 5.9 A plot of extinction coefficient versus wavelength for Cd_{0.2}Zn_{0.8}S sample.

5.2. VARIATION OF EXTINCTION COEFFICIENT WITH WAVELENGTH

A plot of extinction coefficient versus wavelength is shown in figure 5.7 and 5.8 for $\text{Cd}_{0.4}\text{Zn}_{0.6}\text{S}$ and $\text{Cd}_{0.2}\text{Zn}_{0.8}\text{S}$ respectively. Increasing Zn in the sample increased the average extinction coefficient. As the Zn content increased, the effect of annealing on extinction coefficient reduced, however, higher annealing temperatures increased the extinction coefficient. Thus, thermal annealing has increased processes that lead to absorption of more electromagnetic radiation in the samples. This can be observed in the sample ($x = 0.8$) figure 5.8, in which annealing at 100, 200 and 300 °C does not seem to have any appreciable effect on the extinction coefficient as compared with the sample ($x = 0.6$) figure 5.7.

The refractive index and dielectric constants could not be evaluated from Eq. (3.1.5) because the reflectance determined from Eq. (3.1.4) gave negative results when scattering had been ignored. The strong absorbance of the films rendered the interference extrema invisible (figure 5.5), and as a result the Swanepoel method could not also be used.

5.3. PHOTOCONDUCTIVITY RESULTS

A plot of photocurrent against time for samples $\text{Cd}_{0.8}\text{Zn}_{0.2}\text{S}$ and $\text{Cd}_{0.4}\text{Zn}_{0.6}\text{S}$ are given in figure 5.7 and 5.8 respectively. The resistance of the samples measured in the dark were 0.258M Ω , 1.25M Ω , 14M Ω and 9M Ω for sample composition $x = 0.2, 0.4, 0.6$ and 0.8 respectively. Using a DC-Constanter PHYWE power supply, a constant current 0.2A and potential difference 10.6V were set for the experiment, using 1000k Ω standard resistor. Attempts to use a resistor of smaller resistance could not work because no potential difference dropped across it.

With these parameters the photocurrent in figure 5.7 was found to peak around 98 μA whereas that in figure 5.8 peaked around 1.7 μA when the light intensity was about 3.11 W/m^2 . The ratio of photoconductivity and dark conductivity is called the photoresponse. This parameter indicates the suitability of a material for use as a photoactive layer in a solar cell device.

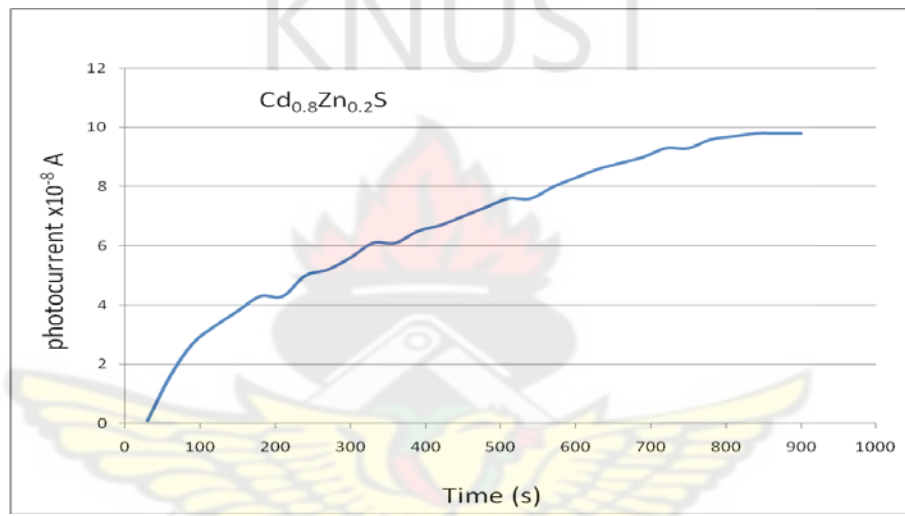


Figure 5.10 A plot of photocurrent versus time for the sample $\text{Cd}_{0.8}\text{Zn}_{0.2}\text{S}$

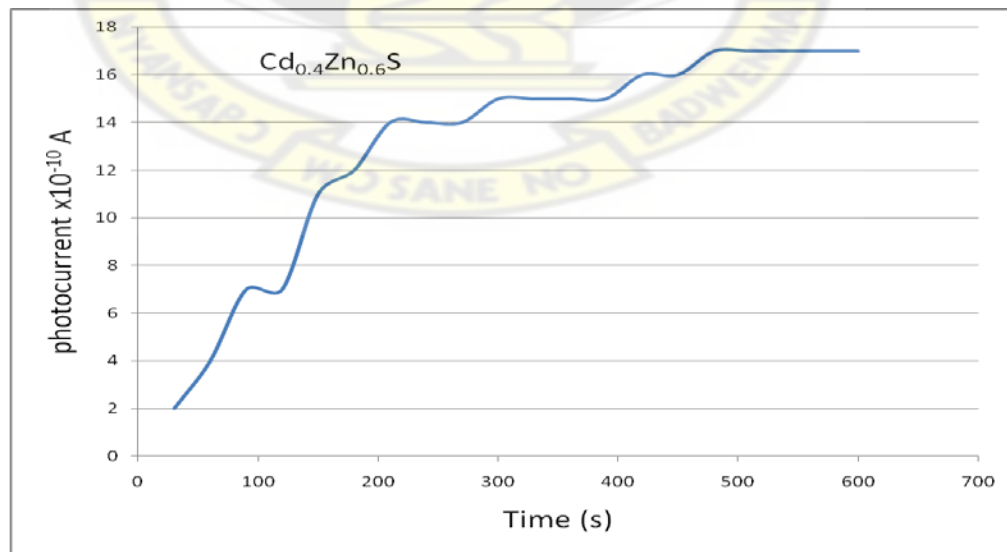


Figure 5.11 A plot of photocurrent versus time for the sample $\text{Cd}_{0.4}\text{Zn}_{0.6}\text{S}$

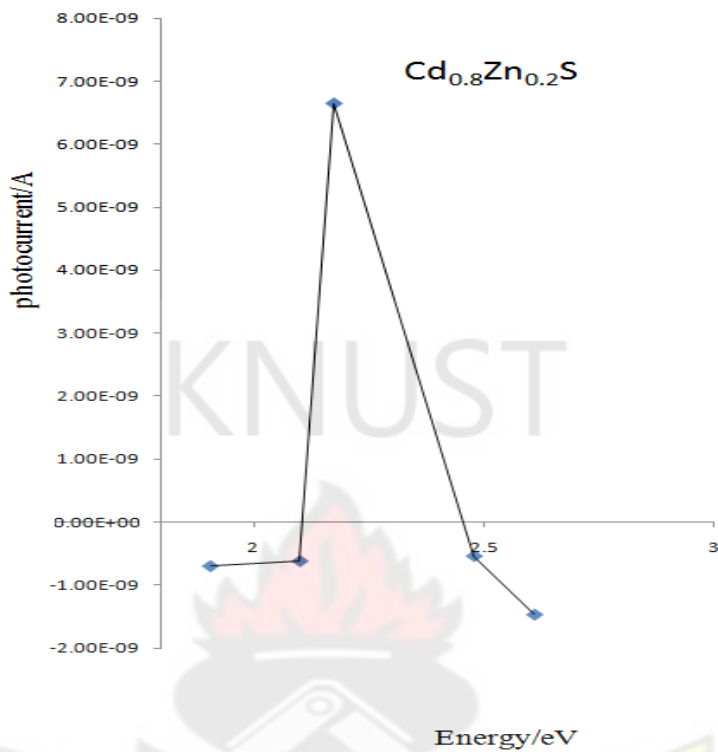


Figure 5.12 A plot of photocurrent versus photon energy for the sample $\text{Cd}_{0.8}\text{Zn}_{0.2}\text{S}$

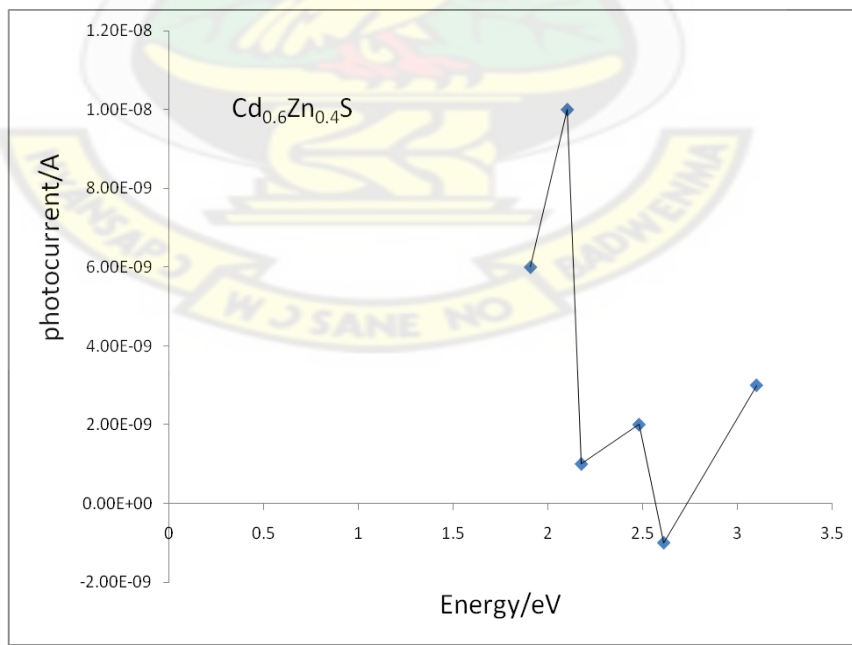


Figure 5.13 A plot of photocurrent versus photon energy for the sample $\text{Cd}_{0.6}\text{Zn}_{0.4}\text{S}$

Also, a plot of photocurrent versus photon energy for the sample $\text{Cd}_{0.8}\text{Zn}_{0.2}\text{S}$ is given in figure 5.8. It was observed that there was a high photoconductivity around 2.20eV photon energy; this is quite close but lower than the corresponding band gap of that sample which was calculated to be 2.42eV, differing by about 0.22eV. Since the films were deposited at high temperature and at a fast rate, they are bound to favour amorphous films. This then indicates that the transition may have occurred from localised states within the band gap rather than transition from valence band to the conduction band. In figure 5.8 for $\text{Cd}_{0.6}\text{Zn}_{0.4}\text{S}$, it seems none of the photon energy used corresponds exactly to the energy of such localised state hence the absence of high photoconductivity, yet still there was a spike at 2.15 eV which may still be due to transition from localised states.

Negative photoconductivity occurred where the illumination decreased the dark conductivity instead of increasing it. Negative photoconductivity has been reported in CdS by (Boer, *et al.*, 1954).

6. CONCLUSIONS AND RECOMMENDATIONS

6.0. CONCLUSIONS

The dip technique used for the preparation of thin films of semiconducting ternary alloy $\text{Cd}_{1-x}\text{Zn}_x\text{S}$ is a relatively simple and low cost method which can be relied on in places where highly specialized equipment for films deposition are lacked. Optical studies of the films revealed that increasing zinc content and annealing temperature all increase the absorbance of the films. Absorbance spectra obtained from the films were used to evaluate the optical band gaps. Band gap of the as deposited films varied from 2.42eV ($x = 0.2$) to 3.61eV ($x = 0.8$), i.e. the band gap increase with increasing Zn concentration of the alloy. These band gap values compare favorably with literature values of similar films. Thermal annealing however decreased the band gap of the samples; this may be due to improved crystalline structure of the samples as a result of the heat treatment. The average extinction coefficient for the as deposited samples were 6.89×10^{-3} , 10.27×10^{-3} , 19.93×10^{-3} , 22.16×10^{-3} for $x = 0.2, 0.4, 0.6, 0.8$ respectively.

The films formed were moderately photoconductive in the as deposited state with photocurrent peaking at 98 μA in the $\text{Cd}_{0.8}\text{Zn}_{0.2}\text{S}$ sample. A high photoconductivity around 2.20 eV photon energy observed in the $\text{Cd}_{0.8}\text{Zn}_{0.2}\text{S}$ sample is quite close but smaller than the corresponding band gap of 2.42 eV of the sample. Transition from localised states within the forbidden gap is speculated to be the cause for high photocurrent.

6.1. RECOMMENDATIONS

In future, access to an X-ray diffractometer will be helpful in revealing more about the structure of the films, that is it will help indicate whether the films are crystalline, polycrystalline or amorphous in nature and also the crystallographic orientation the films as they are they are annealed. Again, XRD will ascertain whether the decrease band gap of the films with thermal annealing is caused by phase transformation or improved crystallinity. Doping with boron by adding boric acid to the solution can be another way to investigate the properties of this ternary alloy.



7. REFERENCES

- AbuShama, J. R. Noufi, S. Johnston, S. Ward, and X. Wu, (2005).** ‘Improved Performance in CuInSe₂ and Surface Modified CuGaSe₂ Solar Cells’, 31st IEEE PVSC, pp. 299-302.
- Adachi, S., (2009).** Properties of Semiconductor Alloys: Group-IV, III-V, and II-VI Semiconductors, pp. 4-5.
- Al Kuhaimi, S.A. and Tulbah, Z., (2000).** Structural, Compositional, Optical, and Electrical Properties of Solution-Grown Zn_xCd_{1-x}S Films. *J. Electrochem. Soc.*, **147**, 214.
- Balkanski, M. and Wallis, R.F., (2000).** Semiconductor Physics and Applications. *Oxford University Press*. Oxford. pp.1-2, 18-19, 68-69.
- Beal, S. E., (1978).** Cleaning and Surface Preparation, *Thin Solid Films*, **53**, 97.
- Bhattacharjee, B., Mandal, S.K., Chakrabarti, K., Ganguli, D., and Chaudhuri, S., (2002).** Optical properties of Cd_{1-x}Zn_xS nanocrystallites in sol-gel silica matrix. *J. Appl. Phys.* **35**, 2636.
- Boer, Borchardt and Borchardt, Z. (1954).** *Phys. Chem.*, **203**, 145.
- Bube, R. H., (1960).** Photoconductivity of Solids. *John Wiley & Son, Inc.* p. 10.
- Chavhan, S.D., Senthilarasu, S. and Soo-Hyoung Lee, (2008).** Annealing effect on the structural and optical properties of a Cd_{1-x}Zn_xS thin film for photovoltaic applications. Elsevier B.V.
- Chopra, K.L., (1969).** Thin Film Deposition Technology, *McGraw Hill*; New York, pp. 55-68.
- Cody, G. D., (1984).** *Semiconductors and Semimetals B*, **21**, 11.
- Chopra, K.I. and Kaur. I., (1983).** Thin Film Device Applications. Plenum, New York.
- Dunlap, W.C., (1961).** Recent Developments in Semiconductors, *J.Chem. Educ.* No.5, **38**, 238-241.
- Dzhafarov, T.D. Ongul, F., and Karabay, I., (2006).** Formation of CdZnS thin films by Zn diffusion. *J. Appl. Phys.* **39**, 3221.
- Gellings, P.J. and Bouwmeester, H. J. M., (1997).** The CRC Handbook of Solid State Electrochemistry, *CRC Press*, p.84.

- Hodes, G., (2002).** Chemical Solution Deposition of Semiconductor Films. New York, pp.3-6.
- Juster, N. J., (1963).** Conduction and Semiconduction, *J.Chem. Educ.* No.9, **40**, 489-496.
- Karanjai, M.K. and Dasgupta, D., (1986).** Preparation and study of sulphide thin films deposited by the dip technique. *Mater. Lett.* **4**, 368-369.
- Kittel, C., (2005).** Introduction to Solid State Physics, Eighth Edition. *John Wiley & Sons, Inc.* p.577
- Korvink, J.G. and Greiner, A., (2002).** Semiconductors for micro- and Nanotechnology an Introduction for engineers, p.40.
- Kumar, V., Singh, V., Sharma, S.K., Sharma, T.P., (1998).** Band gap determination in thick films from reflectance measurements. *Optical Materials*, **11**, 29.
- Lalena, J.N., Cleary, D.A., Carpenter, E.E. and Dean, N.F., (2008).** Inorganic Materials Synthesis and Fabrication. pp 114-115.
- Li, S.S., (2006).** Semiconductor Physical Electronics, Second Edition, pp.246-253, p.335.
- Mattox, D. M., (1978).** Surface Cleaning in Thin Film Technology, *Thin Solid Films*, No. 1, **53**, 81.
- Minami, T., Miyata, T., Ihara, K., Minamino, Y., Tsukada, S., (2006).** *Thin Solid Films*, **494**, 47.
- Neamen, D.A., (2003).** Semiconductor Physics and Devices, Basic Principles, Third Edition, p.2, pp. 144-145.
- Ohring, M., (1992).** The Materials Science of Thin Films, *Academic Press*, San Diego. pp. 195-199, 336-339.
- Ortega-Lopez M., Vigil-Galan, O., Cruz-Gandarilla, F. and Solorza-Feria, O., (2003)** ‘‘Preparation of AgInS₂ chalcopyrite thin films by chemical spray pyrolysis’’, *Materials Research Bulletin*, **38**, 55-61.
- Oztas, M. and Bedir, M., (2001).** Some Properties of Cd_{1-x}Zn_xS and Cd_{1-x}Zn_xS(In) Thin Films Prepared by Pyrolytic Spray Technique. *Journal of Applied Sciences*, **4**, 534-537.
- Padam, G.K., Malhotra, G.L. and Rao, S.U.M., (1988).** *J. Appl. Phys.*, **63**,770.

- Padam, G.K and Rao, S.U.M., (1986)** Preparation and characterization of chemically deposited CuInS₂ thin films, *Sol. Ener. Mater.***13**, 297-305.
- Panin, G.N., Diaz-Guerra, C. and Piqueras, J., (1998).** *Semicond. Sci.Technol.* **13**, 576.
- Pawar, S.H., Tamhanker, S.P. and Lokhande, C.D., (1986).** Studies on electrochemical photovoltaic cells formed with thin film Bi₂CdS₄ Photoelectrodes, *Sol. Ener. Mater.* **14**, 71-77.
- Petterson, J. D. and Bailey, B. C., (2005).** Solid-State Physics Introduction to the Theory, pp.293-294, 113, 637.
- Poole, C.P.Jr., (2004).** Encyclopedic Dictionary of Condensed Matter Physics, vol.1 p. 66, 440, 1391.
- Schroeder, H., (1969).** Oxide layers deposited from organic solutions. *Physics of Thin Films, Academic Press: New York*, **5**, 87-141.
- Singh, J., (2003).** Electronic and Optoelectronic Properties of Semiconductor Structures, *Cambridge University Press; New York*, p. IV, 51-52.
- Singh, J., (2006).** Optical Properties of Condensed Matter and Applications, *John Wiley and Sons, Ltd.* pp.2-4.
- Sole, J. G., Bausa, L. E. and Jaque, D., (2005).** An Introduction to the Optical Spectroscopy of Inorganic Solids, pp. 11-12.
- Sólyom, J., (2008).** Fundamentals of the Physics of Solids, Electronic Properties, Volume II, pp. 89-195.
- Song, J., Li, S. S., Yoon, S., Kim, W. K., Kim, J., Chen, J., Craciun, V., Anderson, T.J., Crisalle, O. D. and Ren, F., (2005).** Growth and Characterization of CdZnS Thin Film Buffer Layers by Chemical Bath Deposition, *IEEE*, 449-451. Also available at <http://ieeexplore.ieee.org/stamp/stamp.jsp?arnumber=01488166>.
- Tauc, J., (1974).** Amorphous and Liquid Semiconductors, Plenum: New York, p. 159.
- Venables, J.A., (2003).** Introduction to Surface and Thin Film Processes, *Cambridge University Press. Cambridge.* pp 5--60.
- Woon-Jo and Gye-Choon, (2003).** Structural and electrical properties of CuGaS₂ thin films by electron beam evaporation, *Solar Energy Materials and Solar Cells*, **75**, 93-100.

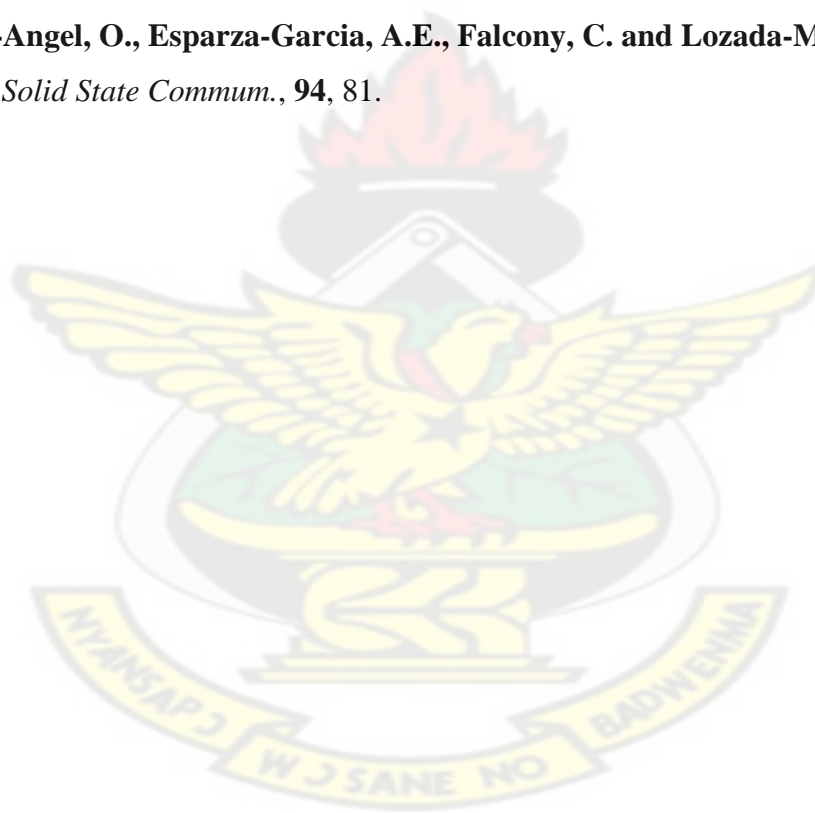
Yacobi, B. G., (2004). Semiconductor Materials an Introduction to Basic Principles, pp.1-3, 154-157, 107.

Yamaguchi, T., Yamamoto, Y., Tanaka, T., Demizu, Y. and Yoshida, A., (1996). Influence of precursor structure on the properties of Cu(In,Ga)Se₂ thin films by thermal crystallization. *Thin Solid Films*, **281/282**, 375.

Yamaguchi, T., Yamamoto, Y., Tanaka, T. and Yoshida, A., (1999). Preparation and characterization of (Cd,Zn)S thin films by chemical bath deposition for photovoltaic devices. *Thin Solid Films*, **344**, 516.

Yokogawa, T., Ishikawa, T., Merz, J.L. and Taguchi, T., (1994). Spectroscopic characterization of band discontinuity in free-standing CdZnS/ZnS strained layer superlattices. *Appl. Phys.* **75**, 2189.

Zelaya-Angel, O., Esparza-Garcia, A.E., Falcony, C. and Lozada-Morales, R., (1995). *Solid State Commun.*, **94**, 81.



8. APPENDICES

8.0. APPENDIX A

Table 5.1 ABSORBANCE READING FOR AS DEPOSITED FILMS

Wavelength /nm	x=0.2	x=0.4	x=0.6	x=0.8
300	3.000	1.568	1.610	1.774
310	3.000	1.503	1.440	1.538
320	3.000	1.379	1.372	1.471
330	3.000	1.259	1.315	1.425
340	3.000	1.230	1.296	1.481
350	3.000	1.216	1.283	1.498
360	3.000	1.179	1.294	1.413
370	3.000	1.130	1.253	1.421
380	3.000	1.113	1.253	1.516
390	3.000	1.121	1.207	1.106
400	3.000	1.104	1.184	1.296
410	3.000	1.082	1.217	1.351
420	3.000	1.045	1.185	1.274
430	3.000	1.012	1.199	1.290
440	3.000	0.964	1.178	1.284
450	2.879	0.977	1.120	1.316
460	2.551	0.913	1.083	1.274
470	2.238	0.879	1.064	1.268
480	1.995	0.837	1.043	1.264
490	1.821	0.823	1.026	1.254
500	1.706	0.791	1.002	1.282
510	1.609	0.778	1.026	1.227
520	1.519	0.754	0.993	1.206
530	1.355	0.747	0.994	1.209
540	1.267	0.684	0.986	1.227
550	1.199	0.667	0.964	1.227
560	1.130	0.665	0.958	1.125
570	1.072	0.686	0.936	1.224
580	1.017	0.694	0.952	1.212
590	0.966	0.665	0.922	1.249
600	0.921	0.687	0.917	1.237
610	0.878	0.623	0.902	1.272
620	0.839	0.660	0.910	1.155
630	0.803	0.627	0.905	1.231

640	0.772	0.660	0.845	1.105
650	0.742	0.695	0.876	1.208
660	0.715	0.644	0.864	1.086
670	0.694	0.640	0.841	1.111
680	0.625	0.655	0.857	1.201
690	0.563	0.604	0.809	1.043
700	0.604	0.620	0.812	1.165
710	0.607	0.614	0.826	1.164
720	0.602	0.606	0.789	1.080
730	0.596	0.608	0.778	1.161
740	0.590	0.599	0.831	1.167
750	0.586	0.571	0.809	1.091
760	0.585	0.587	0.800	1.121
770	0.585	0.594	0.745	1.181
780	0.586	0.572	0.746	1.132
790	0.590	0.541	0.751	1.131
800	0.594	0.578	0.786	1.116
810	0.598	0.541	0.751	1.081
820	0.601	0.558	0.732	1.090
830	0.602	0.561	0.711	1.136
840	0.600	0.561	0.710	1.094
850	0.596	0.527	0.724	1.091
860	0.590	0.561	0.715	1.108
870	0.583	0.537	0.713	1.079
880	0.578	0.497	0.695	1.119
890	0.575	0.537	0.713	1.104
900	0.576	0.549	0.687	1.082

Table 5.2 ABSORBANCE READING FOR FILMS ANNEALED AT 100 °c

Wavelength /nm	x=0.2	x=0.4	x=0.6	x=0.8
300	3.000	3.000	3.000	3.000
310	3.000	2.870	2.890	2.992
320	3.000	2.426	2.458	2.533
330	3.000	3.000	3.000	3.000
340	3.000	2.945	2.960	3.000
350	3.000	2.684	2.721	2.893
360	3.000	2.520	2.582	2.762
370	3.000	2.422	2.505	2.693
380	3.000	2.356	2.458	2.645

390	3.000	2.255	2.381	2.512
400	3.000	2.149	2.288	2.378
410	3.000	2.056	2.206	2.263
420	3.000	1.970	2.126	2.167
430	3.000	1.882	2.048	2.085
440	3.000	1.807	1.985	2.026
450	3.000	1.702	1.884	1.944
460	3.000	1.589	1.779	1.873
470	3.000	1.504	1.724	1.843
480	2.704	1.410	1.670	1.803
490	2.399	1.320	1.612	1.769
500	2.199	1.257	1.561	1.732
510	2.081	1.208	1.516	1.698
520	2.001	1.163	1.475	1.665
530	1.847	1.042	1.354	1.557
540	1.770	0.991	1.303	1.512
550	1.708	0.953	1.266	1.484
560	1.647	0.916	1.230	1.455
570	1.594	0.886	1.200	1.430
580	1.542	0.857	1.170	1.408
590	1.494	0.831	1.144	1.387
600	1.450	0.808	1.120	1.369
610	1.408	0.786	1.097	1.352
620	1.369	0.767	1.076	1.337
630	1.333	0.749	1.057	1.323
640	1.300	0.734	1.040	1.311
650	1.269	0.720	1.024	1.301
660	1.240	0.709	1.010	1.292
670	1.218	0.702	1.002	1.287
680	1.146	0.644	0.942	1.231
690	1.082	0.595	0.891	1.184
700	1.120	0.647	0.941	1.239
710	1.120	0.661	0.952	1.254
720	1.112	0.666	0.955	1.260
730	1.103	0.669	0.956	1.264
740	1.094	0.672	0.957	1.268
750	1.087	0.676	0.959	1.273
760	1.082	0.682	0.963	1.280
770	1.078	0.689	0.968	1.288
780	1.077	0.698	0.974	1.296
790	1.077	0.707	0.982	1.306
800	1.078	0.717	0.989	1.316
810	1.078	0.726	0.997	1.326

820	1.078	0.735	1.003	1.334
830	1.075	0.741	1.007	1.339
840	1.070	0.744	1.007	1.342
850	1.062	0.744	1.006	1.341
860	1.053	0.742	1.002	1.338
870	1.043	0.739	0.997	1.335
880	1.035	0.738	0.993	1.332
890	1.029	0.738	0.992	1.331
900	1.026	0.742	0.993	1.334

KNUST

Table 5.3 ABSORBANCE READING FOR FILMS ANNEALED AT 200 °c

Wavelength /nm	x=0.2	x=0.4	x=0.6	x=0.8
300	3.000	1.963	1.680	3.000
310	3.000	3.000	2.875	2.897
320	3.000	2.687	2.461	2.491
330	3.000	3.000	3.000	3.000
340	3.000	3.000	2.984	3.000
350	3.000	2.915	2.715	2.870
360	3.000	2.739	2.577	2.835
370	3.000	2.625	2.495	2.663
380	3.000	2.556	2.453	2.626
390	3.000	2.447	2.379	2.524
400	3.000	2.338	2.289	2.421
410	3.000	2.240	2.211	2.324
420	3.000	2.149	2.134	2.231
430	3.000	2.056	2.056	2.136
440	3.000	1.981	1.995	2.064
450	3.000	1.877	1.904	1.965
460	3.000	1.780	1.820	1.885
470	3.000	1.709	1.773	1.846
480	3.000	1.615	1.724	1.805
490	3.000	1.503	1.668	1.761
500	3.000	1.412	1.619	1.721
510	2.983	1.343	1.573	1.684
520	2.788	1.287	1.530	1.649
530	2.573	1.160	1.407	1.541
540	2.479	1.103	1.357	1.497
550	2.412	1.061	1.320	1.465
560	2.348	1.021	1.283	1.434

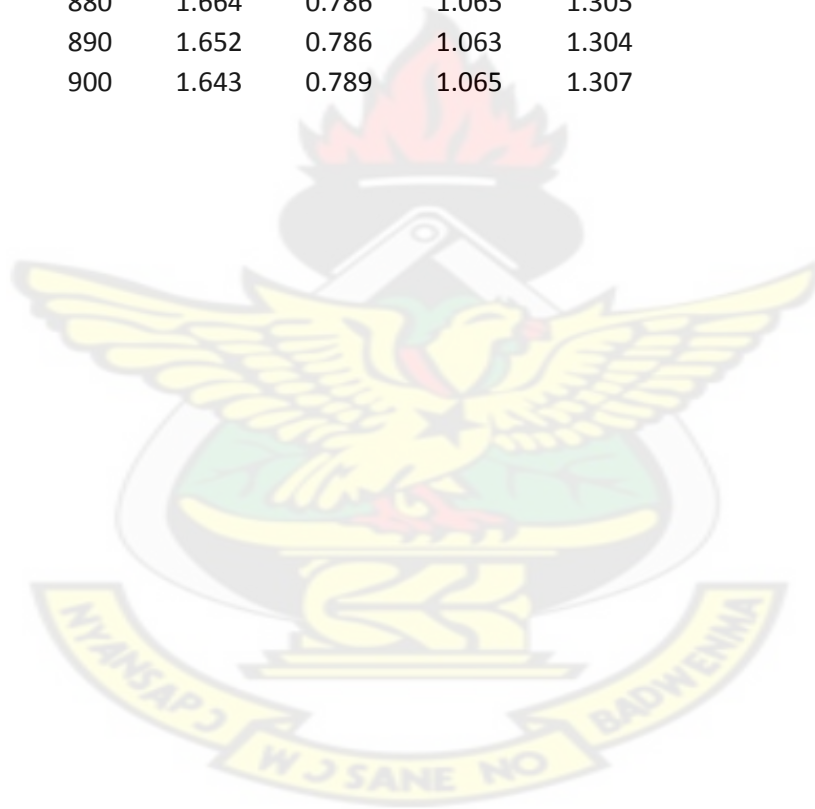
570	2.295	0.987	1.253	1.410
580	2.243	0.936	1.224	1.386
590	2.194	0.926	1.197	1.364
600	2.152	0.902	1.174	1.345
610	2.108	0.877	1.151	1.327
620	2.068	0.856	1.130	1.311
630	2.032	0.837	1.112	1.298
640	2.000	0.820	1.095	1.285
650	1.968	0.804	1.079	1.274
660	1.939	0.790	1.065	1.264
670	1.916	0.781	1.056	1.259
680	1.843	0.723	0.997	1.204
690	1.779	0.671	0.946	1.155
700	1.816	0.722	0.995	1.210
710	1.815	0.735	1.007	1.226
720	1.808	0.738	1.010	1.232
730	1.808	0.740	1.011	1.237
740	1.799	0.742	1.012	1.240
750	1.789	0.745	1.014	1.246
760	1.782	0.750	1.018	1.253
770	1.775	0.756	1.022	1.260
780	1.770	0.763	1.028	1.269
790	1.767	0.772	1.036	1.279
800	1.764	0.781	1.043	1.289
810	1.761	0.790	1.051	1.298
820	1.757	0.798	1.057	1.307
830	1.751	0.802	1.061	1.312
840	1.742	0.804	1.061	1.315
850	1.730	0.803	1.059	1.314
860	1.717	0.801	1.055	1.312
870	1.703	0.798	1.051	1.309
880	1.690	0.795	1.047	1.307
890	1.680	0.794	1.045	1.306
900	1.672	0.797	1.046	1.308

Table 5.4 ABSORBANCE READING FOR FILMS ANNEALED AT 300 °c

Wavelength nm	x=0.2	x=0.4	x=0.6	x=0.8
300	3.000	1.880	1.363	1.742
310	3.000	3.000	2.905	2.927

320	3.000	2.603	2.483	2.527
330	3.000	3.000	3.000	3.000
340	3.000	3.000	2.990	3.000
350	3.000	2.856	2.748	2.881
360	3.000	2.684	2.607	2.746
370	3.000	2.573	2.523	2.673
380	3.000	2.505	2.478	2.641
390	3.000	2.400	2.403	2.540
400	3.000	2.291	2.312	2.434
410	3.000	2.195	2.232	2.338
420	3.000	2.104	2.155	2.245
430	3.000	2.013	2.077	2.151
440	3.000	1.939	2.015	2.080
450	3.000	1.836	1.924	1.981
460	3.000	1.743	1.841	1.900
470	3.000	1.676	1.776	1.859
480	3.000	1.590	1.746	1.816
490	3.000	1.483	1.691	1.771
500	3.000	1.391	1.641	1.729
510	3.000	1.319	1.594	1.691
520	2.948	1.262	1.551	1.655
530	2.708	1.134	1.428	1.544
540	2.605	1.078	1.377	1.499
550	2.532	1.036	1.339	1.467
560	2.461	0.996	1.302	1.436
570	2.401	0.963	1.271	1.409
580	2.343	0.932	1.242	1.385
590	2.288	0.903	1.215	1.363
600	2.241	0.880	1.191	1.344
610	2.191	0.855	1.168	1.326
620	2.146	0.834	1.147	1.309
630	2.105	0.816	1.128	1.295
640	2.065	0.799	1.111	1.283
650	2.028	0.783	1.095	1.271
660	1.993	0.770	1.082	1.261
670	1.965	0.762	1.073	1.256
680	1.888	0.704	1.014	1.200
690	1.817	0.654	0.962	1.153
700	1.850	0.704	1.012	1.207
710	1.845	0.717	1.024	1.222
720	1.832	0.722	1.027	1.229
730	1.817	0.724	1.027	1.233
740	1.802	0.727	1.028	1.237

750	1.789	0.730	1.031	1.242
760	1.779	0.736	1.035	1.249
770	1.769	0.742	1.039	1.257
780	1.762	0.750	1.046	1.266
790	1.757	0.759	1.053	1.276
800	1.752	0.768	1.061	1.286
810	1.747	0.777	1.068	1.296
820	1.740	0.785	1.075	1.305
830	1.732	0.791	1.078	1.310
840	1.721	0.793	1.079	1.313
850	1.708	0.793	1.077	1.313
860	1.693	0.791	1.073	1.310
870	1.678	0.788	1.069	1.307
880	1.664	0.786	1.065	1.305
890	1.652	0.786	1.063	1.304
900	1.643	0.789	1.065	1.307



8.1. APPENDIX B

Table 5.5 Variation of sample composition with optical band gaps evaluated from absorption spectra.

Composition x	E_g (eV)for as-deposited sample	E_g (eV) sample annealed 100°C	E_g (eV) sample annealed 200°C	E_g (eV) sample annealed 300°C
0.2	2.42	2.32	2.14	2.12
0.4	3.36	2.75	2.62	2.60
0.6	3.48	2.52	2.52	2.50
0.8	3.61	2.63	2.63	2.60

Table 5.6 Energy gap for III-V, II-VI, and I-VII semiconductors at room temperature.

III-V compound	ϵ_g (eV)	II-VI compound	ϵ_g (eV)	I-VII compound	ϵ_g (eV)
AlSb	1.63	ZnO	3.20	AgF	2.8
GaP	2.27	ZnS	3.56	AgCl	3.25
GaAs	1.43	ZnSe	2.67	AgBr	2.68
GaSb	0.71	CdS	2.50	AgI	3.02
InP	1.26	CdSe	1.75	CuCl	3.39
InAs	0.36	CdTe	1.43	CuBr	3.07
InSb	0.18	HgS	2.27	CuI	3.11

8.2. APPENDIX C

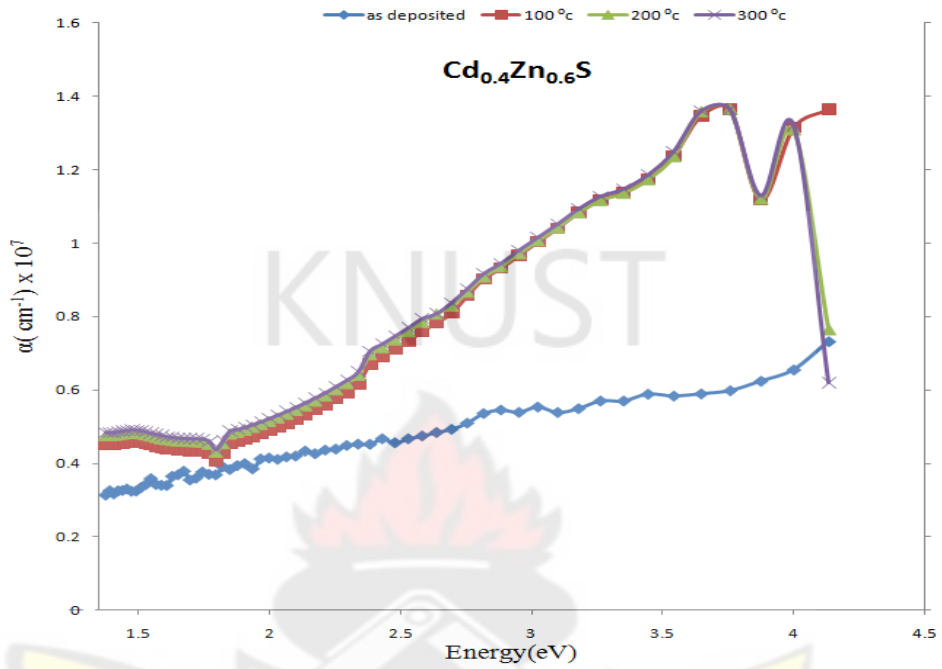


Figure C1 Absorption coefficient, α , versus photon energy, $h\nu$, for $\text{Cd}_{0.4}\text{Zn}_{0.6}\text{S}$ sample.

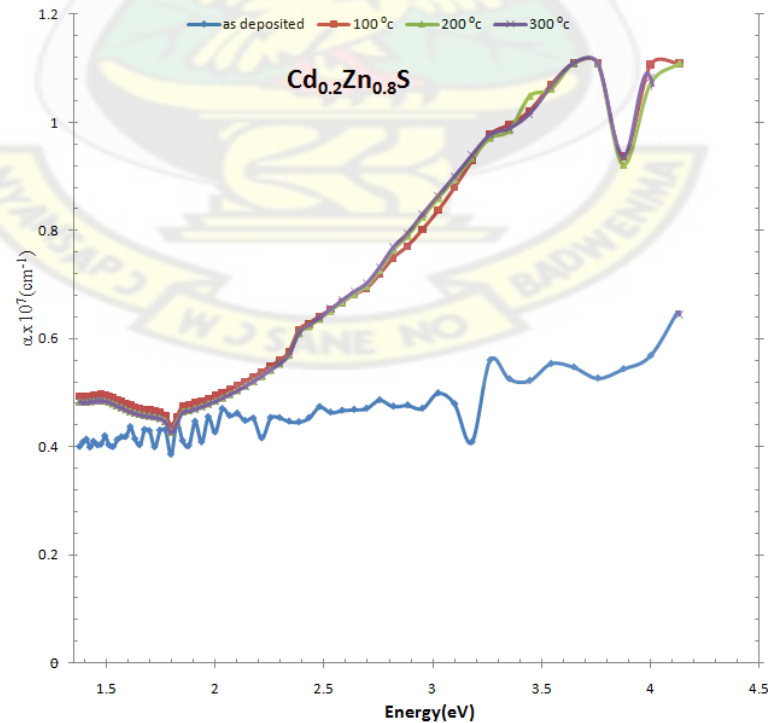


Figure C2 Absorption coefficient, α , versus photon energy, $h\nu$, for $\text{Cd}_{0.2}\text{Zn}_{0.8}\text{S}$ sample.

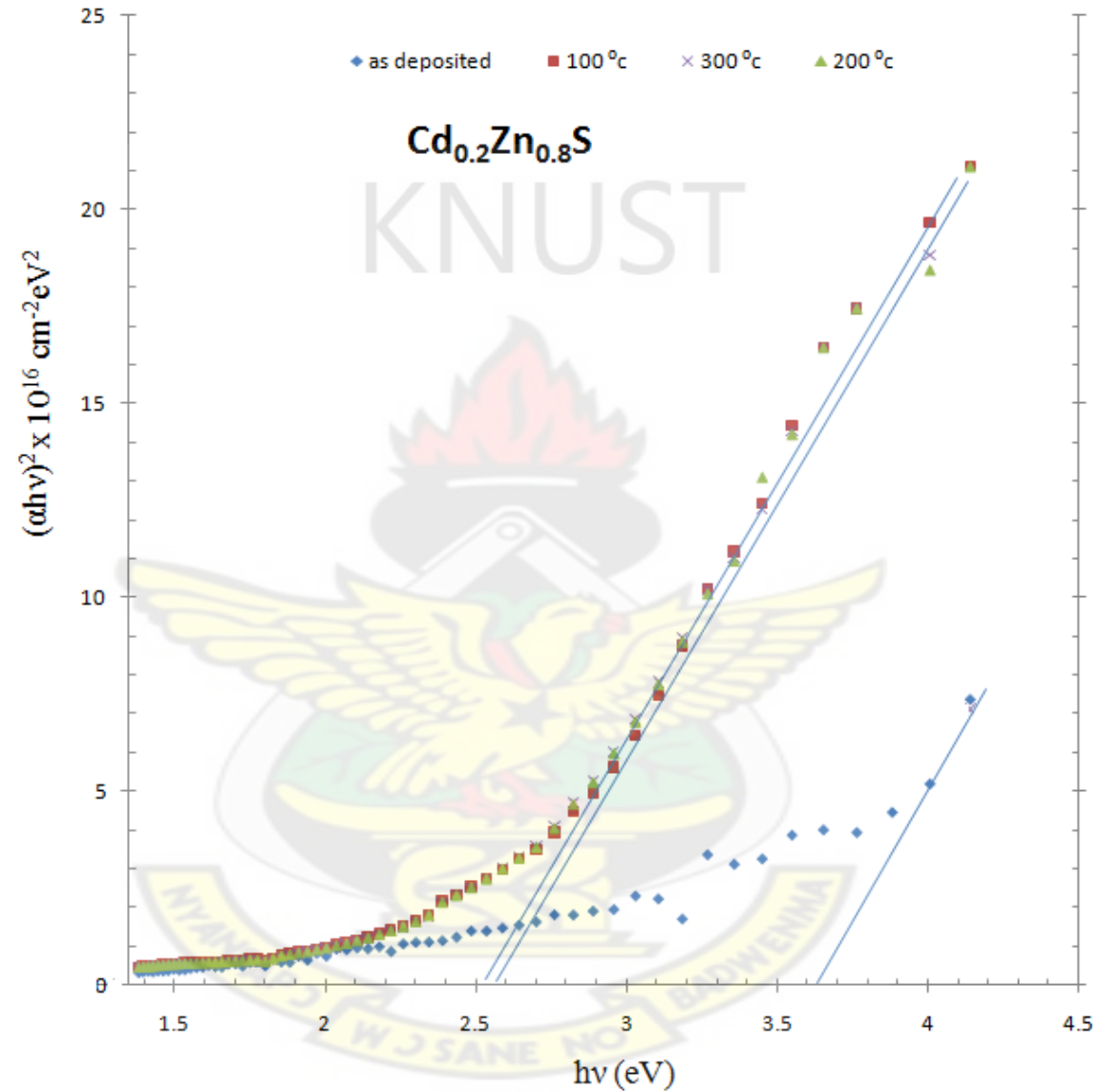


Figure C3 Square of absorption coefficient, α^2 , multiplied by square of photon energy, $(h\nu)^2$, plotted as a function of the photon energy, $h\nu$, for $\text{Cd}_{0.2}\text{Zn}_{0.8}\text{S}$ film annealed at different temperatures. Extrapolation of the straight region of the plot to $(\alpha h\nu)^2 = 0$ gives the optical band gap.

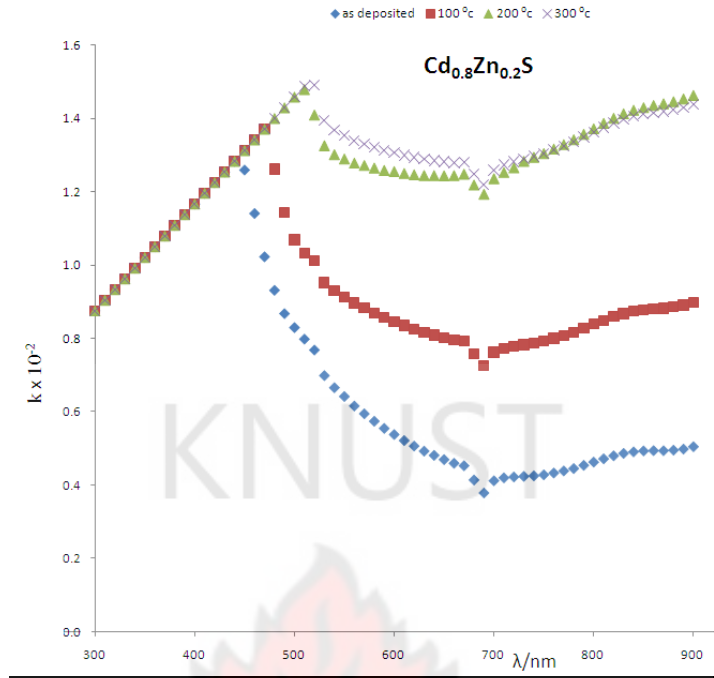


Figure C4 A plot of extinction coefficient versus wavelength for $\text{Cd}_{0.8}\text{Zn}_{0.2}\text{S}$ sample.

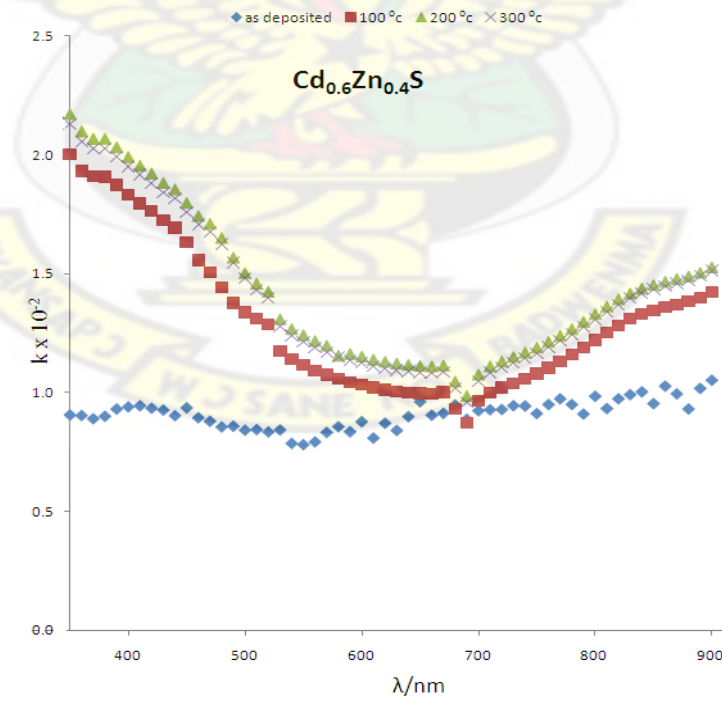


Figure C5 A plot of extinction coefficient versus wavelength for $\text{Cd}_{0.6}\text{Zn}_{0.4}\text{S}$ sample.

8.3. APPENDIX D

Periodic table of elements

18 VIIIA																	
2 He $1s^2$ Helium																	
10 Ne $2s^2 2p^6$ Neon																	
18 Ar $3s^2 3p^6$ Argon																	
36 Kr $3d^{10} 4s^2 4p^6$ Krypton																	
54 Xe $4d^{10} 5s^2 5p^6$ Xenon																	
86 Rn $5d^{10} 6s^2 6p^6$ Radon																	
13 IIIA 14 IVA 15 VA 16 VIA 17 VIIA																	
5 B $2s^2 2p^1$ Boron																	
6 C $2s^2 2p^2$ Carbon																	
7 N $2s^2 2p^3$ Nitrogen																	
8 O $2s^2 2p^4$ Oxygen																	
9 F $2s^2 2p^5$ Fluorine																	
10 Ne $2s^2 2p^6$ Neon																	
13 Al $3s^2 3p^1$ Aluminum																	
14 Si $3s^2 3p^2$ Silicon																	
15 P $3s^2 3p^3$ Phosphorus																	
16 S $3s^2 3p^4$ Sulfur																	
17 Cl $3s^2 3p^5$ Chlorine																	
18 Ar $3s^2 3p^6$ Argon																	
31 Ga $3d^{10} 4s^2 4p^1$ Gallium																	
32 Ge $3d^{10} 4s^2 4p^2$ Germanium																	
33 As $3d^{10} 4s^2 4p^3$ Arsenic																	
34 Se $3d^{10} 4s^2 4p^4$ Selenium																	
35 Br $3d^{10} 4s^2 4p^5$ Bromine																	
36 Kr $3d^{10} 4s^2 4p^6$ Krypton																	
49 In $4d^{10} 5s^2 5p^1$ Indium																	
50 Sn $4d^{10} 5s^2 5p^2$ Tin																	
51 Sb $4d^{10} 5s^2 5p^3$ Antimony																	
52 Te $4d^{10} 5s^2 5p^4$ Tellurium																	
53 I $4d^{10} 5s^2 5p^5$ Iodine																	
54 Xe $4d^{10} 5s^2 5p^6$ Xenon																	
81 Tl $5d^{10} 6s^2 6p^1$ Thallium																	
82 Pb $5d^{10} 6s^2 6p^2$ Lead																	
83 Bi $5d^{10} 6s^2 6p^3$ Bismuth																	
84 Po $5d^{10} 6s^2 6p^4$ Polonium																	
85 At $5d^{10} 6s^2 6p^5$ Astatine																	
86 Rn $5d^{10} 6s^2 6p^6$ Radon																	
11 IB 12 IIB																	
29 Cu $3d^{10} 4s^1$ Copper																	
30 Zn $3d^{10} 4s^2$ Zinc																	
47 Ag $4d^{10} 5s^1$ Silver																	
48 Cd $4d^{10} 5s^2$ Cadmium																	
79 Au $5d^{10} 6s^1$ Gold																	
80 Hg $5d^{10} 6s^2$ Mercury																	
111 Rg $6d^{10} 7s^1$ Darmstadtium																	
112 Copernicium																	
113 Nihonium																	
114 Flerovium																	
115 Moscovium																	
116 Livermorium																	
117 Tennessine																	
118 Oganesson																	
8 9 10																	
26 Fe $3d^6 4s^2$ Iron																	
27 Co $3d^7 4s^2$ Cobalt																	
28 Ni $3d^8 4s^2$ Nickel																	
29 Cu $3d^{10} 4s^1$ Copper																	
30 Zn $3d^{10} 4s^2$ Zinc																	
45 Rh $4d^8 5s^1$ Rhodium																	
46 Pd $4d^{10}$ Palladium																	
76 Os $5d^6 6s^2$ Osmium																	
77 Ir $5d^7 6s^2$ Iridium																	
78 Pt $5d^9 6s^1$ Platinum																	
79 Au $5d^{10} 6s^1$ Gold																	
80 Hg $5d^{10} 6s^2$ Mercury																	
108 Hs $6d^8 7s^2$ Hassium																	
109 Mt $6d^7 7s^2$ Meitnerium																	
110 Ds $6d^9 7s^1$ Darmstadtium																	
111 Rg $6d^{10} 7s^1$ Darmstadtium																	
112 Copernicium																	
113 Nihonium																	
114 Flerovium																	
115 Moscovium																	
116 Livermorium																	
117 Tennessine																	
118 Oganesson																	
3 IIIB 4 IVB 5 VB 6 VIB 7 VIIB 8 VIII 9 VIIIB 10 IIB																	
21 Sc $3d^1 4s^2$ Scandium																	
22 Ti $3d^2 4s^2$ Titanium																	
23 V $3d^3 4s^2$ Vanadium																	
24 Cr $3d^5 4s^1$ Chromium																	
25 Mn $3d^5 4s^2$ Manganese																	
26 Fe $3d^6 4s^2$ Iron																	
27 Co $3d^7 4s^2$ Cobalt																	
28 Ni $3d^8 4s^2$ Nickel																	
29 Cu $3d^{10} 4s^1$ Copper																	
30 Zn $3d^{10} 4s^2$ Zinc																	
39 Y $4d^1 5s^2$ Yttrium																	
40 Zr $4d^2 5s^2$ Zirconium																	
41 Nb $4d^4 5s^1$ Niobium																	
42 Mo $4d^5 5s^1$ Molybdenum																	
43 Tc $4d^5 5s^2$ Technetium																	
44 Ru $4d^7 5s^1$ Ruthenium																	
45 Rh $4d^8 5s^1$ Rhodium																	
46 Pd $4d^{10}$ Palladium																	
73 Ta $5d^3 6s^2$ Tantalum																	
74 W $5d^4 6s^2$ Tungsten																	
75 Re $5d^5 6s^2$ Rhenium																	
76 Os $5d^6 6s^2$ Osmium																	
77 Ir $5d^7 6s^2$ Iridium																	
78 Pt $5d^9 6s^1$ Platinum																	
79 Au $5d^{10} 6s^1$ Gold																	
80 Hg $5d^{10} 6s^2$ Mercury																	
104 Rf $6d^4 7s^2$ Rutherfordium																	
105 Db $6d^5 7s^2$ Dubnium																	
106 Sg $6d^6 7s^2$ Seaborgium																	
107 Bh $6d^7 7s^2$ Bohrium																	
108 Hs $6d^8 7s^2$ Hassium																	
109 Mt $6d^7 7s^2$ Meitnerium																	
110 Ds $6d^9 7s^1$ Darmstadtium																	
111 Rg $6d^{10} 7s^1$ Darmstadtium																	
112 Copernicium																	
113 Nihonium																	
114 Flerovium																	
115 Moscovium																	
116 Livermorium																	
117 Tennessine																	
118 Oganesson																	
1 1A 2 IIA																	
1 H $1s^1$ Hydrogen																	
3 Li $[He] 2s^1$ Lithium																	
4 Be $1s^2$ Beryllium																	
11 Na $[Ne] 3s^1$ Sodium																	
12 Mg $3s^2$ Magnesium																	
19 K $[Ar] 4s^1$ Potassium																	
20 Ca $4s^2$ Calcium																	
37 Rb $[Kr] 5s^1$ Rubidium																	
38 Sr $5s^2$ Strontium																	
55 Cs $[Xe] 6s^1$ Cesium																	
56 Ba $6s^2$ Barium																	
87 Fr $[Rn] 7s^1$ Francium																	
88 Ra $7s^2$ Radium																	
58 Ce $4f^2 6s^2$ Cerium																	
59 Pr $4f^3 6s^2$ Praseodymium																	
60 Nd $4f^4 6s^2$ Neodymium																	
61 Pm $4f^5 6s^2$ Promethium																	
62 Sm $4f^6 6s^2$ Samarium																	
63 Eu $4f^7 6s^2$ Europium																	
64 Gd $4f^7 5d^1 6s^2$ Gadolinium																	
65 Tb $4f^9 6s^2$ Terbium																	
66 Dy $4f^{10} 6s^2$ Dysprosium																	
67 Ho $4f^{11} 6s^2$ Holmium																	
68 Er $4f^{12} 6s^2$ Erbium																	
69 Yb $4f^{14} 6s^2$ Ytterbium																	
70 Lu $4f^{14} 5d^1 6s^2$ Lutetium																	
89 Ac $6d^1 7s^2$ Actinium																	
90 Th $6d^2 7s^2$ Thorium																	
91 Pa $5f^2 6d^1 7s^2$ Protactinium																	
92 U $5f^3 6d^1 7s^2$ Uranium																	
93 Np $5f^4 7s^2$ Neptunium																	
94 Pu $5f^6 7s^2$ Plutonium																	
95 Am $5f^7 7s^2$ Americium																	
96 Cm $5f^7 6d^1 7s^2$ Curium																	
97 Bk $5f^9 6d^1 7s^2$ Berkelium																	
98 Cf $5f^{10} 7s^2$ Californium																	
99 Es $5f^{11} 7s^2$ Einsteinium																	
100 Fm $5f^{12} 7s^2$ Fermium																	
101 Md $5f^{13} 7s^2$ Mendelevium																	
102 No $5f^{14} 7s^2$ Nobelium																	
103 Lr $5f^{14} 6d^1 7s^2$ Lawrencium																	
Lanthanoids																	
Actinoids																	